

OPEN ACCESS

Review—Surface-Enhanced Raman Scattering Sensors for Food Safety and Environmental Monitoring

To cite this article: Haibin Tang *et al* 2018 *J. Electrochem. Soc.* **165** B3098

View the [article online](#) for updates and enhancements.

You may also like

- [High enhancement factor of SERS probe based on silver nano-structures deposited on a silica microsphere by laser-assisted photochemical method](#)
Huy Bui, Thuy Van Nguyen, Thanh Son Pham *et al.*
- [One-step fabrication of fiber optic SERS sensors via spark ablation](#)
Attila Kohut, Viktória Horváth, Zsuzsanna Pápa *et al.*
- [Highly sensitive and stable SERS probes of alternately deposited Ag and Au layers on 3D SiO₂ nanogrids for detection of trace mercury ions](#)
Yi Tian, , Han-Fu Wang *et al.*



Your Lab in a Box!

The PAT-Tester-i-16: All you need for Battery Material Testing.

- ✓ All-in-One Solution with integrated Temperature Chamber!
- ✓ Cableless Connection for Battery Test Cells!
- ✓ Fully featured Multichannel Potentiostat / Galvanostat / EIS!

www.el-cell.com +49 40 79012-734 sales@el-cell.com


electrochemical test equipment





Review—Surface-Enhanced Raman Scattering Sensors for Food Safety and Environmental Monitoring

Haibin Tang,^{1,2,*} Chuhong Zhu,² Guowen Meng,^{2,3,z} and Nianqiang Wu^{1,**,z}

¹Department of Mechanical and Aerospace Engineering, West Virginia University, Morgantown, West Virginia 26506-6106, USA

²Key Laboratory of Materials Physics, and Anhui Key Laboratory of Nanomaterials and Nanotechnology, Institute of Solid State Physics, Chinese Academy of Sciences, Hefei 230031, People's Republic of China

³University of Science and Technology of China, Hefei 230026, People's Republic of China

This article gives a review of surface-enhanced Raman scattering (SERS) sensors for food safety and environmental pollution monitoring. It introduces the basic concepts of SERS substrates, SERS enhancement factors and mechanisms, SERS probes/labels, molecular recognition elements as well as optofluidic SERS devices (SERS sensors integrated with microfluidics). This article places an emphasis on the design strategies of various SERS sensors by utilizing fingerprinting SERS spectra or by using SERS probes. It highlights the applications of SERS sensors in detection of heavy metals (such as Hg²⁺, Pb²⁺, Cd²⁺ and As³⁺), inorganic anions (nitrite, nitrate, perchlorate and fluoride), toxic small molecules (polycyclic aromatic hydrocarbon, polychlorinated biphenyls, herbicides, pesticides, antibiotics and food additives), as well as pathogens (bacteria and viruses).

© The Author(s) 2018. Published by ECS. This is an open access article distributed under the terms of the Creative Commons Attribution 4.0 License (CC BY, <http://creativecommons.org/licenses/by/4.0/>), which permits unrestricted reuse of the work in any medium, provided the original work is properly cited. [DOI: 10.1149/2.0161808jes]



Manuscript submitted February 28, 2018; revised manuscript received April 5, 2018. Published April 21, 2018. *This paper is part of the JES Focus Issue on Ubiquitous Sensors and Systems for IoT.*

Food safety and environment pollution are among great challenges in the human society. There are some common pollutants in the environment and food, such as heavy metals, nitrites, phosphates, pesticides, herbicides, antibiotics, hormone, pathogens and other additives. Some pollutants initially are released into the environment, and then accumulate in the food chain, and enter human bodies. Uptake of pollutants by human poses a threat to human health to different extents.^{1,2} Hence it is essential to monitor pollutants in the environment and food. Currently pollutants are typically measured with various laboratory-based techniques, such as atomic absorption spectroscopy, atomic fluorescence spectrometry, X-ray fluorescence spectrum, inductively coupled plasma and ion-coupled plasma-mass spectroscopy, mass spectrometry, chromatography, capillary electrophoresis, analytical profile index (API), polymerase chain reaction (PCR), and enzyme-linked immunosorbent assay (ELISA).³⁻⁷ Although these techniques have high sensitivity and accuracy, they rely on expensive instruments and require professional to treat samples and operate instruments in centralized laboratories. Additionally, analysis generally takes several hours to days. For example, 0.024 ppb of Hg²⁺ and 0.023 ppb of As³⁺ in drinking water can be detected using atomic absorption spectroscopy with a two-step electrothermal atomizer and hydride generation atomic fluorescence spectrometry, respectively.^{8,9} However, they need multiple sample preconcentration processing and expensive instruments. PCR can improve the number of the target while ELISA can produce amplified recognition signal, which could both improve the detection sensitivity to pathogens. For example, oligonucleotide microarray with combination of CdSe/ZnS quantum dots as fluorescent labels shown high specificity and sensitivity of 10 colony forming units (CFU)/mL.¹⁰ However, the complicated procedures are very time-consuming, and the method is also vulnerable to contamination. These laboratory-based techniques cannot meet the critical need of rapid on-site measurement of pollutants. Therefore, it is essential to develop portable sensors for rapid field-deplorable detection so that pollutants can be treated in a timely manner to reduce the possible losses of properties and life.

Researchers have been developing various sensors such as colorimetric, electrochemical, acoustic, fluorescent, infrared, surface-enhanced Raman scattering (SERS) and field-effect transistor (FET)

devices.¹¹⁻¹⁴ Colorimetric sensors are inexpensive and easy to operate, but generally cannot be used for quantification of analyte due to their low sensitivity. Fluorescent sensors have high sensitivity and good for quantitative analysis.^{14,15} Currently most of fluorescent sensors are operated in the visible-light spectral range, which makes it difficult to be used in complex sample matrix due to the interference. Electrochemical sensors are inexpensive and compact, but suffer from non-specific adsorption and fouling of electrodes in complex sample matrix. It is convenient to use electrochemical sensors to detect metal ions, but complicated to construct immunoassays based on electrochemistry. SERS sensors emerged in 1990s and were developed rapidly in the last two decades because SERS sensors has unique features as compared to other portable devices. First of all, it is a vibrational spectroscopy method, which provides the fingerprint information of analytes. Second, water molecules have no interference on the SERS signal. Third, SERS has deep penetration depth in complex sample matrices such as milk, fruit juices and blood when a near-infrared light is employed as an excitation source. Therefore, SERS sensors have a great promise in food safety and environment monitoring.

The details of SERS history,¹⁶⁻¹⁸ enhancement mechanism,^{19,20} and applications in chemistry,^{21,22} bioscience,^{23,24} and medical sciences can be found in other review articles.^{25,26} In food safety or environment monitoring field, a few of review papers are focused on SERS detection of pathogen bacteria,²⁷ mercury,^{28,29} pesticide residues,^{30,31} arsenic,³² perchlorate,³³ and other targets in food safety issues.^{12,34,35} This review article will place an emphasis on design of SERS sensors for food safety and environment monitoring, depending on different types of analytes, such as inorganic ions, small molecules and pathogens.

SERS Signal Amplification and Analyte Capture

SERS substrates.—Raman scattering is extremely inefficient due to the small scattering cross section of $\sim 10^{-30}$ cm²/molecule, which is about 14 orders of magnitude lower than the cross sections of fluorescent dye molecules.³⁶ Therefore, it is essential to use SERS substrates that are able to enhance Raman signals to achieve high sensitivity of SERS sensors. Generally SERS substrates are designed according to two enhancement mechanisms: chemical enhancement (CE) and electromagnetic (EM) enhancement. It has been reported that CE can occur in two cases.^{19,37-39} In the first case, the CE effect is typically induced by the charge transfer between the SERS substrate

*Electrochemical Society Student Member.

**Electrochemical Society Fellow.

^zE-mail: nick.wu@mail.wvu.edu; gwmeng@issp.ac.cn

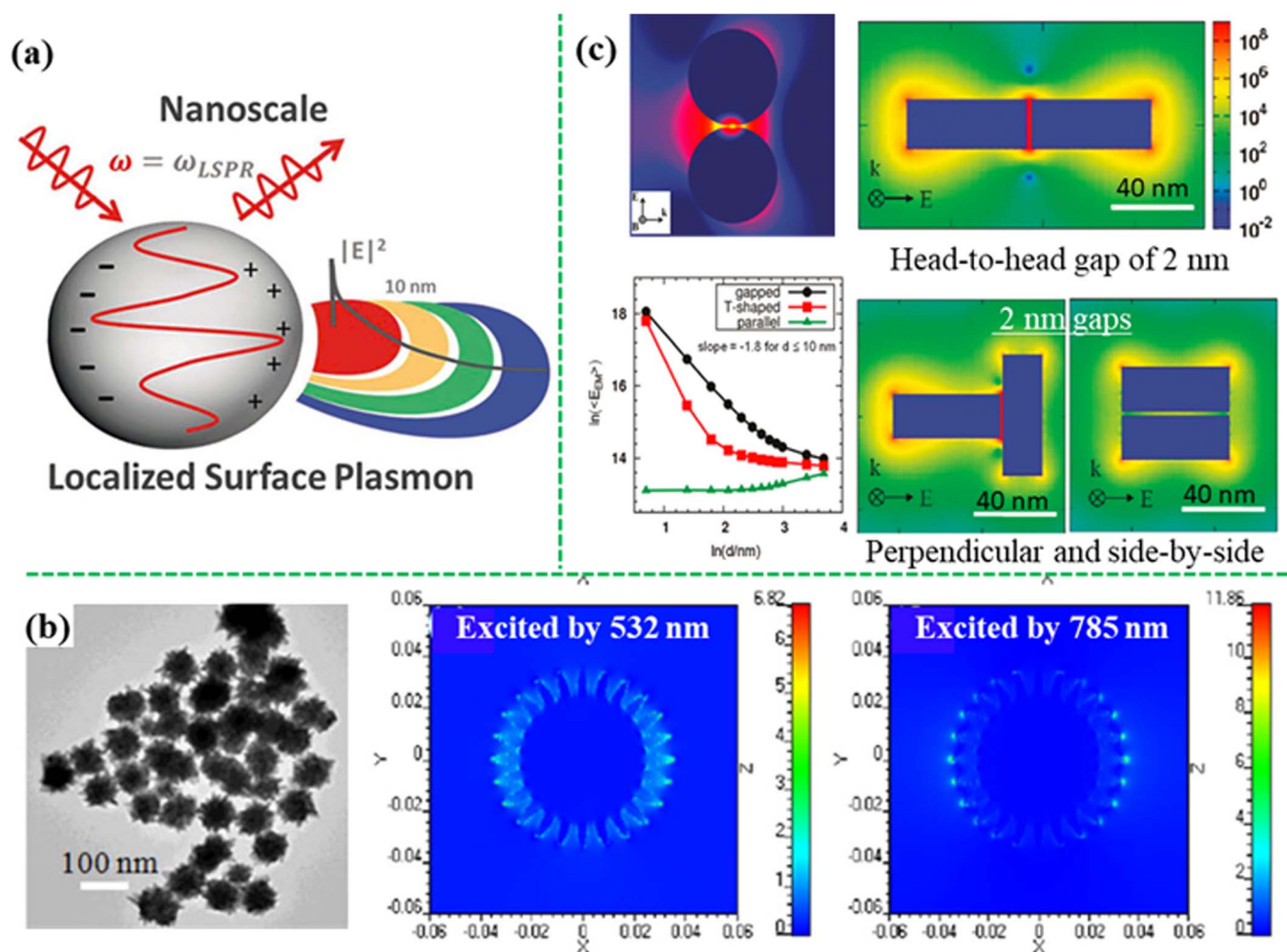


Figure 1. (a) The LSPR-induced local EM field and the decay (modified by permission of The Royal Society of Chemistry).¹⁴ (b) Finite-difference time-domain (FDTD) simulated EM field distributions of nanostar showing “hot spots” surrounding sharp tips (modified by permission of IOP Publishing Ltd).⁴⁶ (c) EM enhancement obtained from discrete dipole approximation (DDA) calculations at the gaps of silver sphere dimer and rod dimers as a function of gap size (modified by permission of American Chemical Society).⁴⁷ The SERS activity increases significantly with a decrease in the gap distance.

and the molecules chemically adsorbed. The charge transfer (the electronic coupling) introduces new states in the electronic structure of the metal-adsorbate complex, which is also called “charge-transfer states”, leading to an increase in the Raman probability (σ_{abs}^R) of the adsorbate. This increases the Raman scattering. The new charge-transfer states could be in resonance with incident light, which could further amplify SERS signal. In the second case, when the Fermi level of metal matches either the lowest unoccupied molecular orbital (LUMO) or the highest occupied molecular orbital (HOMO) of adsorbate, photo-induced charge transfer will occur either between the LUMO and the occupied state below the Fermi level, or between the HOMO and the unoccupied state above the Fermi level. However, the CE effect is typically ineffective given that the enhancement factor is usually less than 100. It is worth noting that the CE mechanism is still somewhat controversial and not understood completely.

EM enhancement originates from the enhanced localized electromagnetic field in plasmonic metal nanostructures. For example, metal (Au, Ag, Cu and Al) nanoparticle with the size comparable or smaller than the wavelength of incident light, localized surface plasmon resonance (LSPR) can be excited with a resonance frequency as^{14,40–42}

$$\omega_{LSPR} = \frac{\omega_p}{\sqrt{1 + 2\varepsilon_{diel}}} \quad [1]$$

The ε_{diel} is the dielectric constant of surrounding medium and the ω_p is the plasma frequency of bulk metal which is given by

$$\omega_p = \sqrt{\frac{ne^2}{m_{eff}\varepsilon_0}} \quad [2]$$

in which n is the density of electrons, m_{eff} is the effective mass, e is the charge of an electron and ε_0 is the permittivity of free space. The important material criteria for enabling strong plasmon and SERS are that the real part of the dielectric function is negative while the imaginary part (denote the damping) is small at the interested wavelength range (typically the visible and near infrared).¹⁹ These lead to the selection of silver and gold as the SERS substrate materials. Among them, silver has the strongest plasmon for the identical structure with shorter LSPR wavelength compared to gold and copper, while gold has better chemical stability and biocompatibility. In the regard of important structural design criteria for strong plasmon and SERS, creating high density of “hot spots” and tuning the LSPR in resonance with the excitation light are effective to achieve highly active SERS substrates.

As shown in Figure 1a, the localized electromagnetic field is pronounced in a very thin zone (~ 10 nm) from the surface of plasmonic nanostructures and decays exponentially.¹⁴ When Raman-active molecules are located in the enhanced electromagnetic field, the intensity of incident light that excites Raman mode of the molecule is

enhanced. Also, the Raman scattering light from the molecule will be enhanced by the same localized electromagnetic field. When both the excitation light and the Raman scattering light are in resonance with the frequency of the LSPR, the SERS signal is maximized, leading to the $|E|^4$ enhancement. Indeed, a shift in the frequency between the excitation light and the Raman scattering light is smaller than the width of the LSPR band. Hence the excitation light and the Raman scattering light can gain the same EM enhancement approximately.

The SERS signal intensity (P_{SERS}) can be estimated under the effects of both the chemical enhancement and electromagnetic enhancement^{37,38}

$$P_{SERS} \propto \text{chemical enhancement} \times \text{EM enhancement} \quad [3]$$

$$P_{SERS} \propto N \cdot \sigma_{abs}^R \cdot |A(v_e)|^2 \cdot |A(v_s)|^2 \cdot I(v_e) \quad [4]$$

where N is the number of adsorbed molecules that experience SERS; $A(v_e)$ and $A(v_s)$ is the excitation light and the Raman scattering light enhancement factors, respectively; $I(v_e)$ is the intensity of excitation light. In this equation, chemical enhancement mainly contributes to σ_{abs}^R . The effect of CE on $I(v_e)$ is rare and negligible even though the CE-induced photons might affect $I(v_e)$ as mentioned in several reports. EM enhancement contributes to $A(v_e)$ and $A(v_s)$. In case of EM enhancement only, the SERS enhancement factor (EF) is determined by

$$EF_{EM} = \frac{P_{SERS}}{P_{0,SERS}} = |A(v_e)|^2 \cdot |A(v_s)|^2 \quad [5]$$

where $P_{0,SERS}$ is the SERS intensity in the absence of EM enhancement. EM enhancement can achieve a SERS EF of $\sim 10^{10}$. This indicates that EM is much larger than chemical enhancement. Hence EM is dominant while the CE effect is minor or negligible in most cases. Furthermore, the EM effect is generally applied to all Raman-active molecules without selectivity. In contrast, chemical enhancement effect is molecule-specific in case of the physicochemical interaction of the molecules with the SERS substrate.¹⁹

Since $|A(v_e)|^2 \sim |E|^2$, an $|E|^2$ approximation can be considered. Furthermore, if ignoring the Raman shift (that is, $\omega_e \sim \omega_s$, where ω_e , ω_s is frequency of the excitation light and Raman scattering light, respectively), the SERS EF due to the EM effect can be approximated¹⁹

$$EF_{EM} = \frac{|E(\omega_e)|^4}{|E_o(\omega_e)|^4} \quad [6]$$

In experiments, the SERS EF can be estimated by

$$EF = \frac{I_{SERS}/N_{SERS}}{I_{Norm}/N_{Norm}} \quad [7]$$

where I_{SERS} , I_{Norm} is the intensity of a specific characteristic peak in the SERS and normal Raman measurements, respectively; N_{SERS} , N_{Norm} is the number of molecules contributing to the Raman signal in the SERS and normal Raman measurements, respectively.⁴³

“Hot spots”.—“Hot spots” for SERS are defined as the area where great EM enhancement exists. First, “hot spots” appear on the regions with sharp edges or corners, which can concentrate the electric field distribution.^{44–46} As shown in Figure 1b, the sharp tips (less than 10 nm in diameter) of the Au nanostars can generate much higher local EM field than other spots with bigger radius of curvature. Second, “hot spots” can be created in the small gaps (<10 nm) between closely spaced plasmonic nanostructures, where plasmon are coupled with each other.^{47,48} As shown in Figure 1c, the small gaps (2 nm) between the neighboring Ag nanospheres and neighboring Ag nanorods can generate high local EM field as the “hot spots”. The SERS activity is highly dependent on the space distance of the gaps.^{49,50} For example, when the gap size decreases from 5.5 nm to 1 nm, the SERS enhancement will improve from $\sim 10^6$ to 10^{11} .^{51–55} Consequently, when analyte molecules are adsorbed on “hot spots”, SERS signals of the analyte can be enhanced by 10^6 or even up to 10^{11} .^{51,56,57} As a result,

even a single molecule can be detected by SERS sensor.⁵⁸ Therefore, one of strategies for sensitivity improvement is to create high-density of “hot spots” over a large area on the SERS substrate. Free-standing colloidal nanoparticles can induce SERS “hot spots” by aggregation in liquid.^{59–62} However, the particle aggregation in liquid is difficult to control, which makes it challenging in reproducibility. To achieve signal uniformity and reproducibility, large-area ordered nanostructures are desirable. Periodic nanostructure arrays on solid substrates have been developed using self-assembly,^{63–69} electrodeposition,^{70–73} template-assisted fabrication,^{74–89} lithography,^{70,90–95} and skeleton-assisted methods.^{96–105}

Resonance with excitation light.—When LSPR band is overlapped the wavelength of the excitation light, that is, the plasmon is in resonance with the excitation light, it can enhance SERS activity. Fortunately plasmonic band can be tuned by tailoring the material component, size, shape of metal nanoparticles and the medium around the metal.¹⁴ For example, increasing the particle size will induce red-shift of the SPR peak (Figure 2a).^{106–108} Compared with sphere-like structures, anisotropic structures show multiple LSPR bands (Figure 2b).⁴⁶ For example, nanorods show two separated plasmon absorption peaks corresponding to the transverse and the longitudinal modes, respectively.^{109,110} The longitudinal mode is sensitive to the aspect ratio, which can be tuned from visible light to infrared light regions (Figure 2c).^{111–116} The LSPR peak can also be tuned by the component of materials, such as the relative ratio of gold to silver in the AuAg alloy (Figure 2d).^{117,118} Additionally, the periodical parameter, i.e. the distance between the neighboring nanostructures can also change the SPR peaks.¹¹⁹

Analyte capture and recognition.—The SPR-induced local EM field enhancement decays exponentially with the distance from the plasmonic metal surface (Figure 1a). Generally, the strongly enhanced EM field is within 10 nm surrounding a plasmonic nanostructure. Therefore, the analyte molecules or SERS labels should be in a proximity to the surface of the SERS substrate to achieve high sensitivity of sensor. A maximum EM enhancement is achieved when analyte molecules or SERS labels are located on “hot spots”. As a result, if the analytes are not apt to be adsorbed (chemically or physically) on the surface, extra capture strategies are needed, which will be discussed in detail in Detection of small molecules section. On the other hand, SERS signal can be turned on or turned off by controlling the distance between analytes and SERS substrate surface, which will be discussed in detail in SERS Sensor Design and Applications section.

Some of analytes are SERS-active. In this case, fingerprinting SERS band of analytes can be used to recognize analytes, which makes it unnecessary to use molecular recognition elements (MREs) in SERS sensors, simplifying the design of sensors. When analytes are not SERS-active, or there is no any fingerprinting SERS band, MREs along with the SERS probes/labels are required for the construction of sensors, in which MREs are used to selectively capture and recognize analytes, achieving specificity, and SERS probes/labels are employed to transduce sensing signals. MREs include antibodies, aptamers, small molecules, molecular imprinted polymers and etc.

SERS probes.—There are typically three types of SERS probes, including (i) the Raman reporter molecules alone, (ii) the plasmonic metal nanoparticles conjugated with Raman reporters, and (iii) the sandwiched metal nanoparticle@Raman reporter@silica nanoparticles, as illustrated in Figure 3. When detecting trace analytes, Raman reporter molecules alone generate weak or no sensing signal. Hence Raman reporter molecules must be close to a SERS substrate after capturing analytes. To solve this problem, bare plasmonic gold or silver nanoparticles functionalized with Raman reporter molecules have been developed as the SERS probes for sensor construction. Such Raman reporter dyes typically contain -SH or -NH₂ moieties because their high affinity to silver or gold substrate, including 4-aminothiophenol (4-ATP), 4-mercaptobenzoic acid (4-MBA), 4-mercaptopyridine. (4-MPY), rhodamine 6 G (R6G), mala-

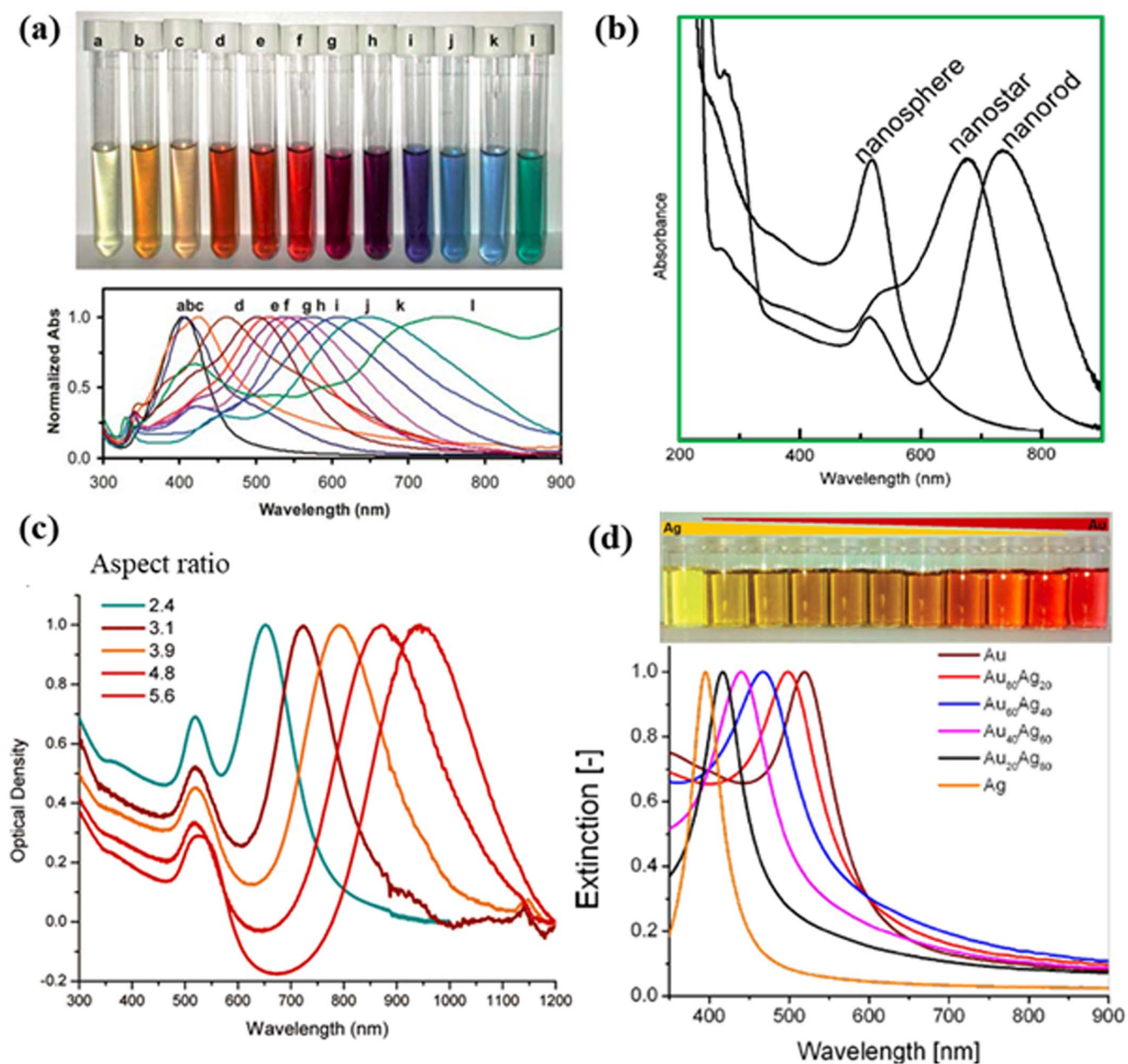


Figure 2. Dependence of LSPR band on the size, shape, aspect ratio, and composition of nanoparticles. (a) Optical photograph and UV-vis absorption spectra of silver colloids with different size and shape (modified by permission of The Royal Society of Chemistry).¹⁰⁸ (b) UV-vis absorption spectra of gold nanospheres, nanorods and nanostars (modified by permission of IOP Publishing Ltd).⁴⁶ (c) SPR spectra of gold nanorods with different aspect ratios, showing the sensitivity of the longitudinal band to the aspect ratio (modified by permission of American Chemical Society).¹¹³ (d) SPR related to the ratio of gold to silver in the AuAg alloy (modified by permission of The Royal Society of Chemistry and Rehbock et al.).^{117,118}

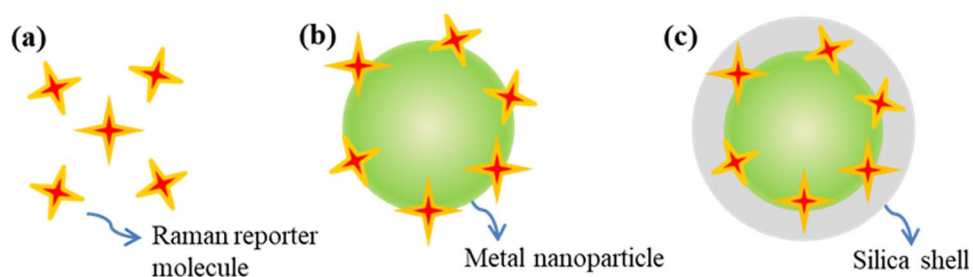


Figure 3. Three kinds of SERS probes used in indirect detection, including (a) the Raman reporter molecules alone, (b) the plasmonic metal nanoparticles conjugated with Raman reporters, and (c) the sandwiched metal nanoparticle@Raman reporter@silica shell nanoparticles.

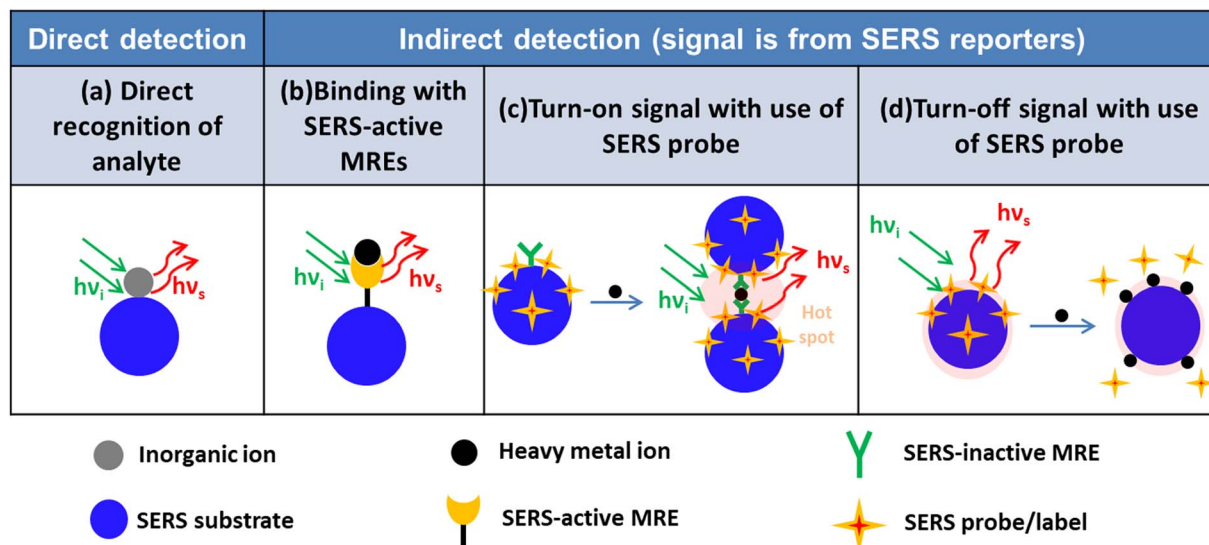


Figure 4. Illustration of different SERS sensor design strategies for inorganic ion detection. (a) Direct recognition of analyte; (b) binding with SERS-active MREs; (c) turn-on signal with use of SERS probe; (d) turn-off signal with use of SERS probe.

chite green isothiocyanate (MGITC), and 5,5-dithiobis-2-nitrobenzoic acid (DTNB). Unfortunately, such SERS probes typically suffer from leaching out of Raman reporter molecules and aggregation in liquid, especially in a solution with high ionic strength. This leads to poor repeatability of detection. To solve this problem, the Raman reporter (MGITC) have been sandwiched between a gold core and a silica shell to form the gold nanostar@MGITC@silica composite nanoparticles as the SERS probes.⁴⁶ Embedding of an abundant of Raman reporter molecules inside a single SERS probe entity not only improves the sensitivity but also prevents from leaching out of Raman reporter molecules. The plasmonic gold nanostar core can significantly enhance the SERS intensity of Raman reporter molecules. The silica shell not only renders the water solubility but also provides a platform for further bio-conjugation. In particular, such SERS probes show excellent dispersion and stability in aqueous solution with high ionic strength.⁴⁶ Therefore, the sandwiched gold nanostar@MGITC@silica SERS probes are characteristic of excellent water-solubility, high sensitivity and good repeatability, which hold a great promise in SERS sensors.

SERS Sensor Design and Applications

Detection of inorganic ions.—Motivation.—There are two categories of harmful inorganic ions in food and environmental contamination: heavy metal cations and toxic anions. They are released into the environment from both natural actions, such as volcanic emissions and interaction of metal-rich rocks with ground water, as well as from industrial and human activities, such as mining and subsequent milling processes, combustion of coals, chemical and electronics manufacturing, solid waste incineration, and food processing. Heavy metals ion, such as arsenic (As^{3+}), mercury (Hg^{2+}), lead (Pb^{2+}), chromium (Cr^{6+}), cadmium (Cd^{2+}) and copper (Cu^{2+}), can cause a variety of human diseases and even death with low concentrations because they accumulate in organisms but are not degraded easily.^{120–123} For example, arsenic causes severe skin damages, circulatory systems problems and increased cancer risk.^{124,125} Mercury can cause permanent brain and kidney damage with serious clinical symptoms such as deafness, visual impairment and cognitive disorders.¹²⁶ Lead can induce high blood pressure and kidney problems for adults; and it is particularly harmful to children, resulting in lower intelligence quotient, hyperactivity, slowed growth in physical or mental development, hearing problems, anemia, and kidney damage.¹²⁷ Human intake of heavy metal ions is mainly from drinking water and the contaminated food. The United States Environmental Protection Agency (EPA) has en-

acted a maximum residue limits in drinking water for heavy metals, such as 10 ppb arsenic, 2 ppb mercury, 15 ppb lead, 5 ppb cadmium, 100 ppb chromium, and 1.3 ppm copper, respectively.¹²¹

Nitrite (NO_2^-), nitrate (NO_3^-), perchlorate ions (ClO_4^-) and fluoride (F^-) are the main harmful inorganic anion contaminants in environment and food. Besides nitrate and nitrite ions naturally occur in soils and water as part of the earth's nitrogen cycle through vegetable and animal decomposition, nitrification by bacteria in aerobic environments and human activities. Production of munitions and explosives also induce excessive nitrate and nitrite. Nitrate can accelerate eutrophication in aquatic environment and consequently disturb or even jeopardize the ecosystem.¹²⁸ The perchlorate can disrupt iodide uptake in the thyroid gland, resulting in thyroid hypertrophy or hyperplasia, which ultimately would lead to hypothyroidism.¹²⁹ Fluoride is beneficial to reducing tooth decay at recommended values (1.5 mg/L). However, it can cause discoloration of tooth enamel at slightly higher consumption levels and serious adverse skeletal effects at higher than about 14 mg/L per day as reported by World Health Organization (WHO).¹³⁰ Besides intake from drinking water, contaminated food is also the intake source according to the survey by U.S. Food and Drug Administration (FDA).¹³¹ EPA has set an enforceable standard, which is called a maximum contaminant level (MCL) in water for nitrates at 10 ppm and for nitrites at 1 ppm.¹³² Health Canada and various states in the United States commends a drinking water guidance value for perchlorate from 1 ppb to 18 ppb.¹²⁹

Sensor design strategies.—Figure 4 shows the different strategies for SERS detection of inorganic ions. Monoatomic heavy metal ions cannot be directly detected by SERS sensors because there are no chemical bonds to generate Raman scattering.¹³³ As a result, only inorganic oxyanions and few oxycations can be directly detected by their characteristic Raman vibration bands. Otherwise, building specific chemical bonds with the heavy metal ions or using extrinsic SERS probes are needed for SERS detections.

Direct recognition of analyte with SERS spectra.—Arsenic, including arsenate (As^{5+}) and arsenite (As^{3+}), can be directly detected by SERS based on the characteristic vibration of As–O bond.³² Meng et al. have revealed that arsenic ions were adsorbed on the silver surface through formation of bidentate binuclear surface complexes ($\text{AgO}_2\text{AsO}_2^-$ via extended X-ray absorption fine structure investigation.¹³⁴ For As^{5+} , two characteristic SERS bands are shown: an intense peak in the range of 780–812 cm^{-1} assigned to the ν_1 (A_1) symmetric As–O stretch mode, and a broad minor peak at $420 \pm 10 \text{ cm}^{-1}$ induced by superposition of the ν_2 (A_1) and ν_5 (E) stretching modes. For

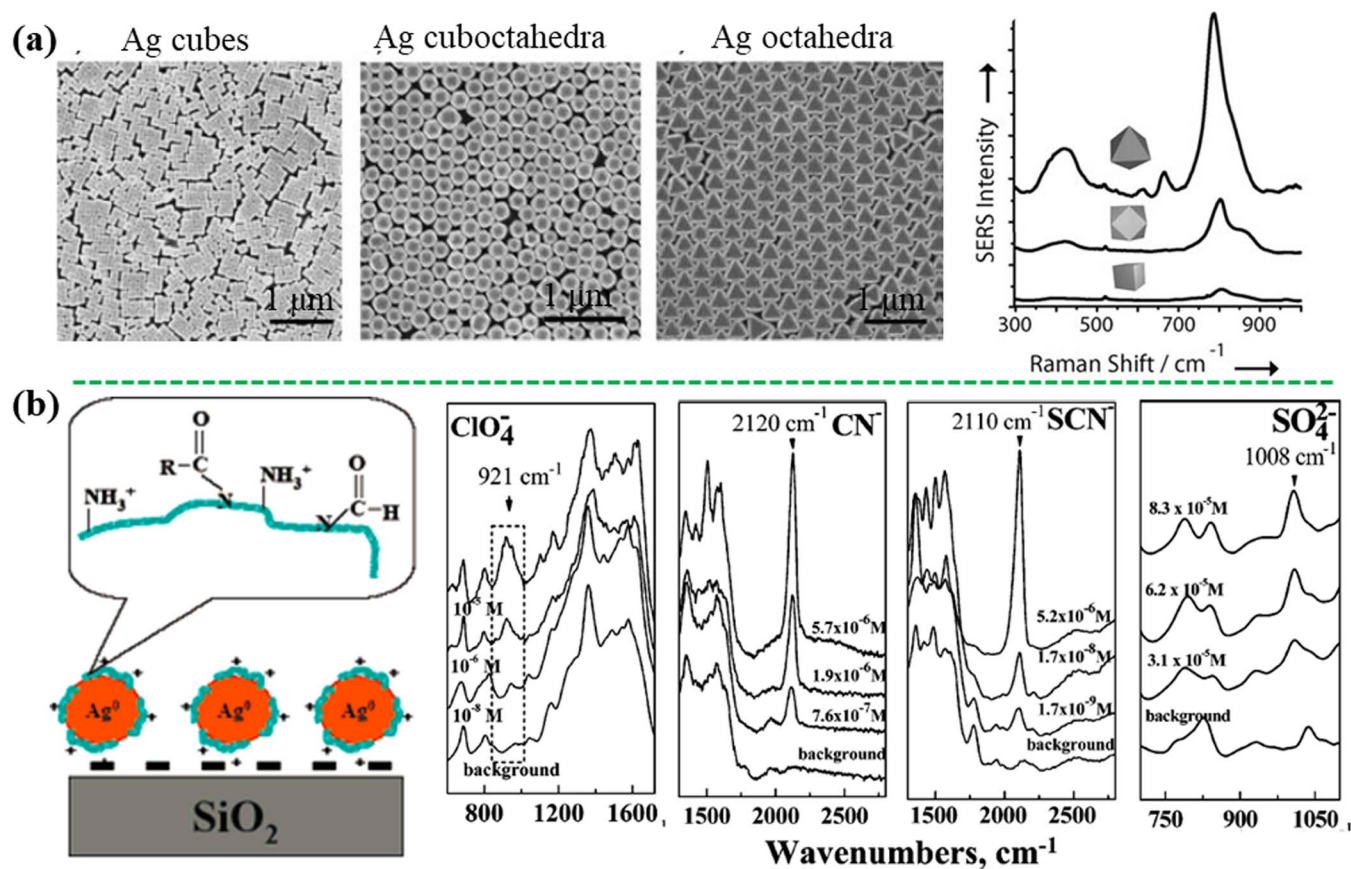


Figure 5. (a) Direct detection of arsenate based on the characteristic peaks at 800 and 425 cm⁻¹ using close-packed self-assembly films of silver nanocubes, nanocubooctahedra, and nanooctahedra (modified by permission of Wiley-VCH).¹³⁵ (b) Positively charged Ag-NPs immobilized on glass substrate showing direct SERS response to anions including ClO₄⁻, CN⁻, SCN⁻, and SO₄²⁻ (modified by permission of American Chemical Society).¹⁴²

As³⁺, two characteristic SERS bands assigned to the same stretching modes in the range of 721–750 cm⁻¹ and around 439 cm⁻¹.³² Based on these, Yang et al. have fabricated the silver nano-arrays by the Langmuir–Blodgett assembly method (Figure 5a) for detection As³⁺ and As⁵⁺. “Hot spots” occurred at the neighboring gaps among the silver nanoparticles (Ag-NPs) and showed high SERS sensitivity, which result in a low limit of detection (LOD) of 1 ppb, an order of magnitude below the standard set by EPA and WHO.¹³⁵ In addition, Meng et al. have employed the silver nanoparticle film and the self-assembled silver nanowire substrates for SERS detection of arsenic species including As⁵⁺ and As³⁺ with LOD from 5 ppb to 10 ppb.³² It is worth mentioning that the position of the characteristic bands depended on the SERS substrate, the excitation wavelength and the experimental condition. Similarly, other oxycations such as uranyl (UO₂²⁺) and neptunyl ions (NpO₂²⁺), can also be directly detected by SERS.^{136,137}

Typically, inorganic oxyanions can be directly detected using SERS with the characteristic vibrational bands in the oxyanions. For example, ClO₄⁻ is directly detected by the SERS characteristic vibration bands at 950 cm⁻¹ (dehydrated) and 934 cm⁻¹ (in aqueous solution) on the Ag nanofilm deposited on a Cu foil.¹³⁸ NO₃⁻ and NO₂⁻ have been directly detected at a LOD of 0.5 ppm by the unique SERS peaks at 1056 and 1326 cm⁻¹, respectively, using the commercial gold-coated silicon substrate.¹³⁹ The Raman cross-sections of these inorganic oxyanions are not large, and their affinity with SERS substrates is remarkably low. As a result, a positive charged layer can be decorated on the surface of SERS substrates to enhance the affinity and the resulting detection sensitivity. Electrostatic attraction by a positively charged layer, such as cystamine¹⁴⁰ and 2-dimethylaminoethanethiol,¹⁴¹ is used to lower the LOD to 1 nM for ClO₄⁻

detection. As shown in Figures 5b, the positively charged Ag-NPs revealed high SERS sensitivity to thiocyanate (SCN⁻), ClO₄⁻, cyanide (CN⁻), and SO₄²⁻ at LOD of 1 ppb, 8 ppb, 7 ppb, and 4 ppm, respectively, due to the synergistic effect of the electrostatic, hydrogen bonding, and dispersive interactions toward anions from the amino and amide groups on the nanoparticle surface.¹⁴²

Binding metal ions with SERS-active MREs.—Indirect detection strategies have been applied to monoatomic heavy metal cations. An effective solution is that SERS-active molecules are employed as the MREs to capture and recognize the specific analyte and to transduce the sensing signal. The first method is to detect the relative change in the vibration bands of the SERS-active MRE after the interaction with heavy metal ions, where this type of SERS-active MRE also serves as the SERS probe. Typically, the plasmonic nanostructure is functionalized with a specific SERS-active MRE, which can coordinate with the metal ions. The unchanged bands of the MRE can work as an internal standard to realize the quantitative detection. For example, the gold nanoparticles (Au-NPs), which were functionalized with trimercaptotriazine (TMT) MRE, were aggregated after adding a very small amount of a sodium chloride solution, inducing the “hot spots” for amplifying the SERS signal. Owing to the specific binding of the metal ions with the third S and two heterocyclic N atoms in the TMT molecule, it provided quantitative assays for Hg²⁺ and Cd²⁺ ions using the intensity ratio of selected vibrational bands in the SERS spectra (Figures 6a and 6b).¹⁴³ Similarly, inorganic Hg²⁺ and methylmercury (CH₃Hg⁺) have been detected at a low LOD of 250 pM by the Au-NPs on polystyrene microbeads, which were functionalized with a monolayer of 4-MPY, where MPY was a SERS-active MRE (Figure 6c).¹⁴⁴ Complexation of Hg²⁺ and CH₃Hg⁺ to the N atom of the MPY ring induced a change in the characteristic bands

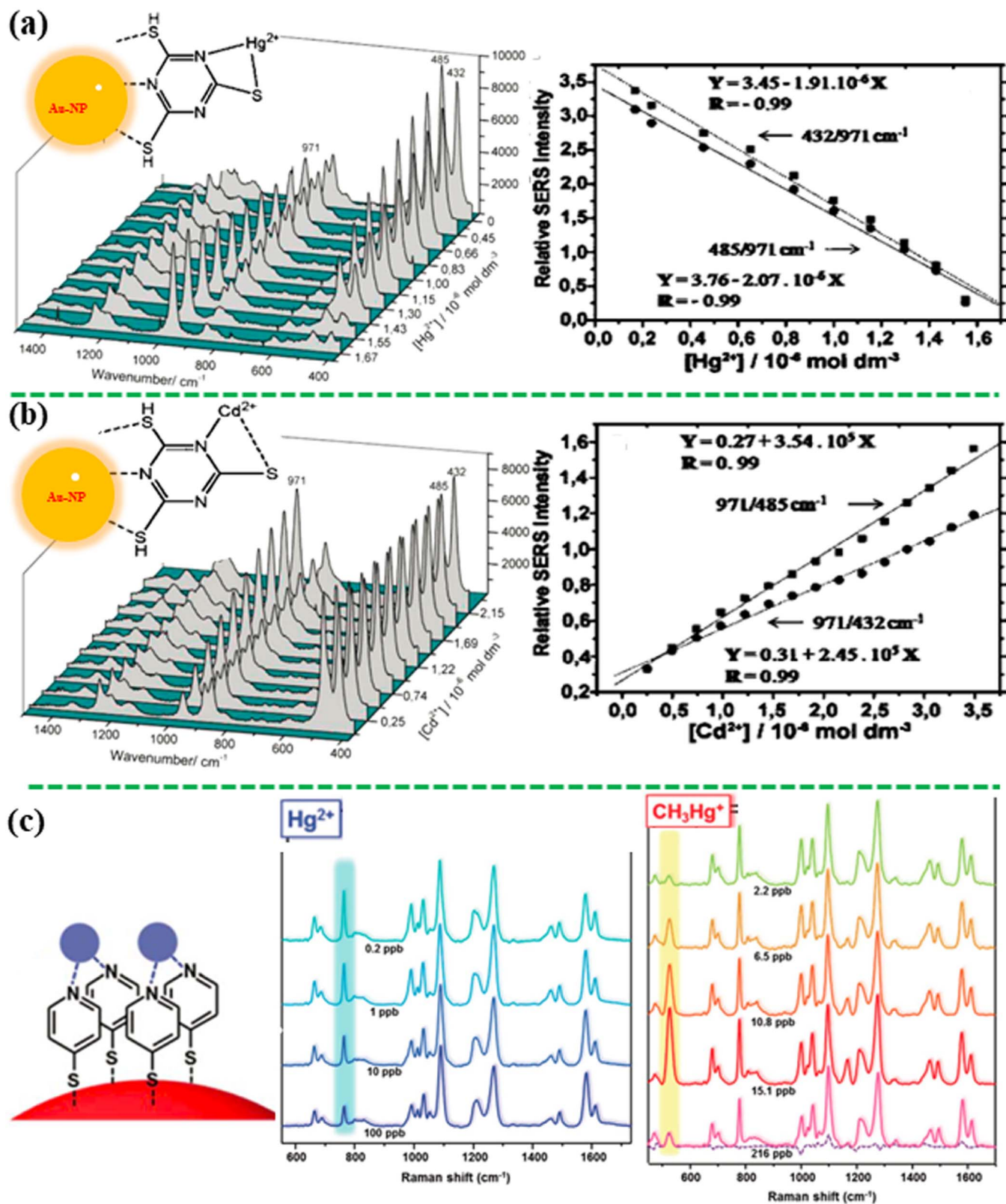


Figure 6. Detection of metal ions using the SERS-active molecular recognition elements (MREs) that binds with metal ions, showing the spectral profile change of MRE with concentration of heavy metal ions. (a) The intensity ratios at 432/971 and 485/971 cm^{-1} versus the concentration of Hg^{2+} and (b) at 971/485 and 971/432 cm^{-1} versus the concentration of Cd^{2+} from the TMT-AuNP aqueous suspension (modified by permission of American Chemical Society).¹⁴³ (c) MPY anchored Au-NPs for detection of Hg^{2+} and CH_3Hg^+ based on intensity ratios of I_{777}/I_{1096} and I_{526}/I_{1096} , respectively (modified by permission of The Royal Society of Chemistry).¹⁴⁴

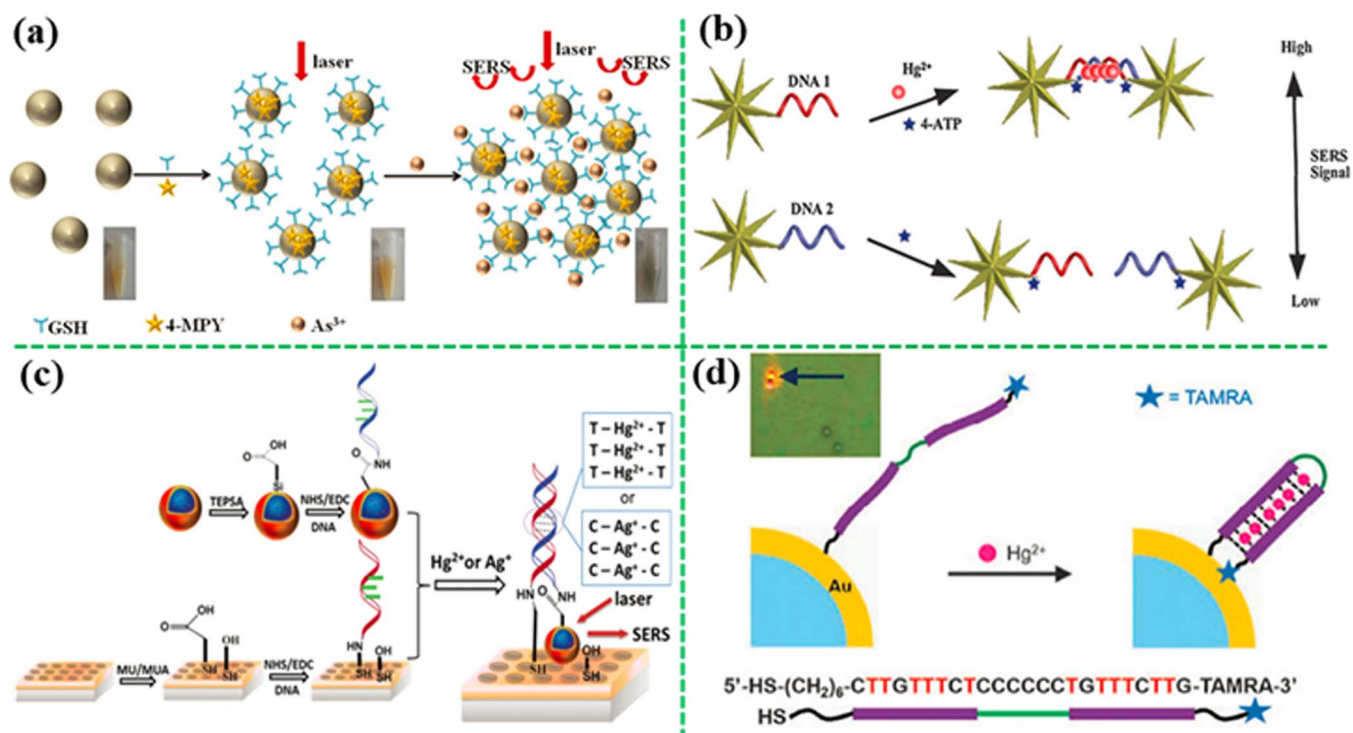


Figure 7. Detection of heavy metal ions by the “turn-on” strategies with use of SERS probes. (a) Aggregation induced by binding of target metal ions with molecular recognition element (MRE) anchored on Ag-NPs (modified by permission of American Chemical Society),¹⁵² and (b) DNA hybridization of two complementary single stranded DNA anchored on gold nanostars¹⁶² or (c) the SERS probes coupled with a gold nanohole array (modified by permission of The Royal Society of Chemistry),¹⁶³ (d) Shortening the distance of SERS probe from the plasmonic structure by change in aptamer conformation (modified by permission of Royal Society of Chemistry).¹⁶⁴

of MPY at 777 cm^{-1} and 526 cm^{-1} , respectively. Normalized by the ring breathing of SERS band at 1096 cm^{-1} , quantitative detection has been realized, where the intensity ratios of the peaks of 777 and 526 cm^{-1} to 1096 cm^{-1} increased with an increase in the Hg^{2+} and CH_3Hg^+ concentrations, respectively. Di-(2-picolyl)amine (DPA) can also worked for this strategy.¹⁴⁵ At the presence of Hg^{2+} , the previous peak at 1060 cm^{-1} became stronger with increasing the Hg^{2+} concentration, realizing the quantitative detection of Hg^{2+} by the intensity ratio of 1060 cm^{-1} peak to 1020 cm^{-1} peak whose intensity is not affected by Hg^{2+} . The other SERS-active MREs for heavy metals, such as 4-(N-piperazinyl) terpyridine dithiocarbamate,¹⁴⁶ 2-mercaptobenzimidazole^{147,148} and 4-MBA,^{149,150} have been anchored on different SERS substrates to detect Zn^{2+} , Cu^{2+} and Pb^{2+} ions, respectively. Recently, Guselnikova et al. have reported that the diethylenetriaminepentaacetic acid (DTPA) functionalized gold grating array demonstrated the selective detection of various heavy metal ions (LOD of 10^{-14} M), such as Hg^{2+} , Pb^{2+} , Cd^{2+} , Co^{2+} and Cu^{2+} .¹⁵¹ DTPA could entrap the heavy metal ions from the solution, leading to pronounced Raman shift of the carbonyl vibrational band at $1515\text{--}1600\text{ cm}^{-1}$, depending on the atomic number of heavy metal ions, enabling the selective detection in the mixture of metal ions.

“Turn-on” signal with use of SERS probe.—If both the analyte and the MRE are not SERS-active, a SERS probe/label will be added into the sensor to transduce the sensing signal. In the “turn-on” sensing principle, the signal of SERS probe is switched on when an analyte is present in an assay; and the SERS intensity increases with an increase in the concentration of analyte. For example, As^{3+} ions were detected by glutathione (GSH)/4-MPY-modified Ag-NPs at a LOD of 0.76 ppb .¹⁵² Figure 7a shows the MPY molecules (SERS probes) and the GSH molecules (MREs) bound to the Ag NP surface. When As^{3+} ions were added to the assay, the As^{3+} ions bound with GSH anchored on the surface of Ag-NP. Binding of As^{3+} with GSH resulted in the aggregation of Ag-NPs, which created “hot spots” between the neighboring Ag NPs, turning on the sensing signal of the SERS probe (MPY). Sim-

ilarly, various MREs, such as chelating polymer,¹⁵³ cysteine,¹⁵⁴ 2,5-Dimercapto-1,3,4-thiadiazole,¹⁵⁵ tetramethyl-rhodamine (TAMRA)-labelled aptamer,¹⁴⁵ polyaromatic ligands,¹⁵⁶ polyaniline,¹⁵⁷ 1,4-diethynylbenzene,¹⁵⁸ and MBA,¹⁵⁹ have been reported for quantitatively and selectively detecting Cr^{6+} (LOD = 1.45 nM),¹⁶⁰ Cd^{2+} ($1\text{ }\mu\text{M}$), Hg^{2+} (1 pM), and Cu^{2+} (10 pM), respectively.

Besides small molecules, DNA is also an effective MRE for metal ions. For example, strong interaction of Hg^{2+} with thymine (T) and Ag^+ with cytosine (C) in the DNA chain result in the formation of the T- Hg^{2+} -T and the C- Ag^+ -C pairs, respectively.^{161,162} Kuang’s group has constructed a SERS sensor for Hg^{2+} detection by turning on the sensing signal through DNA hybridization, achieving a LOD of 4 pM (Figure 7b).¹⁶² In their design, two T-rich single stranded DNA were anchored on the gold nanostars firstly. The Hg^{2+} ions and the SERS probe (4-ATP) were added into the assay. Once the Hg^{2+} ions were present, the two DNA strands were hybridized because of formation of T- Hg^{2+} -T, resulting in self-assembling of gold nanostars into dimers. This made the SERS probes (4-ATP) on the gold nanostars exposed to the “hot spots”, which tuned on the SERS signal. In addition, Wu’s group has coupled a SERS probe (the sandwich gold nanostar@Raman-reporter@silica NP) with an ordered gold nanohole array pattern via DNA hybridization (Figure 7c), and realized the detection of Ag^+ and Hg^{2+} in human saliva at a LOD of 1.7 pM and 2.3 pM , respectively.¹⁶³ As compared to the colloid-suspension assays, the chip-based SERS sensor showed higher sensitivity and better repeatability. Besides double-stranded DNA, single-stranded DNA (aptamer) has been used as the MRE for heavy metal ion detection as well. For example, Chung’s group has reported an aptamer-modified gold microshell for Hg^{2+} detection at LOD of 50 nM (Figure 7d).¹⁶⁴ A long aptamer linked to a SERS probe at the far end was anchored on the surface of gold microshell firstly. Once the Hg^{2+} was present in the assay, the aptamer was folded into a hairpin structure because of the formation of T- Hg^{2+} -T, bringing the SERS probe close to the gold microshell with less than 10 nm , turning on the SERS signal.

Similarly, an aptamer-modified Au-NP@silicon nanowire array showed a low LOD of 1 pM for Hg^{2+} by formation of the hairpin structure in the presence of Hg^{2+} .¹⁶⁵

“Turn-off” signal with use of SERS probe.—In the “turn-off” sensing principle, the SERS probes/reporters are initially close to a plasmonic nanostructure. The SERS reporters’ SERS signal becomes diminished during capture of analytes; and the SERS reporters’ signal intensity decreases with an increase in the concentration of analyte. It can be realized in three ways: (i) pushing the SERS probes away from the plasmonic nanostructure, (ii) reducing the number of the SERS probe on the plasmonic nanostructure, or the number of “hot spots”, and (iii) deactivating the plasmonic metal.

Figure 8a shows that the SERS probes were attached to the surface of a plasmonic gold popcorn.¹⁶⁶ After Hg^{2+} ions were added into the assay, the SERS probe- Hg^{2+} complex was formed, and detached away from the plasmonic nanostructure, which reduced the SERS signal with increasing the Hg^{2+} concentration. Similarly, the 4,4'-dipyridyl (Dpy) functionalized Au@Ag nanoparticles on silicon substrate was developed to detect Hg^{2+} at a LOD of 10 fM.¹⁶⁷ Other SERS probes, such as R6G,^{168,169} methimazole¹⁷⁰ and 2-mercaptoethanesulfonate,¹⁷¹ have been applied for this strategy. Another typical example is shown in Figure 8b.¹⁷² At the initial state, a plasmonic gold nanostructure was functionalized with Aptamer 1, being paired with a complementary Aptamer 2 with one end linked with a SERS probe. The SERS probe was close to the gold nanostructure initially, showing strong SERS signal. When Hg^{2+} ions were present, Aptamer 2 bound with the Hg^{2+} ions, and formed a hairpin structure, leading to dissociation of Aptamer 2 with Aptamer 1. This moved the SERS probe away from the gold nanostructure. Using the similar strategy based on the gold nanowires on a gold film,¹⁷³ Hg^{2+} , Ag^+ and Pb^{2+} were detected simultaneously at LOD of 500 pM, 1 nM, and 50 nM, respectively. These two studies along with other reports showed that aptamers and double-stranded DNA were effective for design of SERS sensors based on the “turn-off” mechanism.^{172–175}

The “turn-off” mechanism can also work by reducing the number of plasmonic nanoparticles.¹⁷⁶ The Au-NPs/rGO initially showed strong SERS signal of rGO (bands at $\sim 1350\text{ cm}^{-1}$ and 1610 cm^{-1}) initially. The presence of Pb^{2+} ions induced detachment of the gold NP away from the rGO sheet due to the dissolution of Au-NP by $\text{S}_2\text{O}_3^{2-}$ and O_2 . Detachment of the Au-NPs away from the rGO surface reduced the SERS signal of rGO. This SERS sensor was able to detect Pb^{2+} with a linear range from 5 nM to 4 μM at a LOD of 1 nM. Figure 8c shows a SERS sensor based on the competitive absorption.¹⁷⁷ Initially, rhodamine B (RB) was immobilized on the Au NPs, showing high SERS intensity. When the Hg^{2+} ions were present in the assay, RB molecules were released from the surface of Au NPs due to the stronger competitive adsorption of Hg^{2+} via electrostatic interaction, reducing the SERS signal. This SERS sensor showed a LOD of 0.5 ppb toward Hg^{2+} . Additionally, the Hg^{2+} ions could be reduced to Hg^0 atoms by reductant (like citrate) anchored on the plasmonic structures and subsequently attached on the surface of the plasmonic structures. This led to deactivation of SERS performance due to the SERS-inactive effect of mercury, besides detachment of SERS probe molecules from the surface of plasmonic structures, reducing the SERS signal. This sensing principle was also demonstrated with the citrate-reduced Ag-NPs and the Au-NPs with different SERS probes.^{178–180}

Detection of small molecules.—*Motivation.*—Small molecules (usually lower than 900 daltons in molecular weight) in environment and food include polycyclic aromatic hydrocarbon (PAHs), polychlorinated biphenyls (PCBs), herbicides, pesticides, antibiotics, various chemicals from industrial wastewater and illegal food additives. PAHs and their derivatives are produced by the incomplete combustion of organics partly from natural combustion such as forest fire and volcanic eruption, but mostly from anthropogenic emissions like combustion of fossil fuels.^{181–185} PAHs are found in water, air, sediment, soil, and food, showing highly toxic, mutagenic and/or carcinogenic effect to both animals and human.^{186,187} PCBs are produced in industrial scale

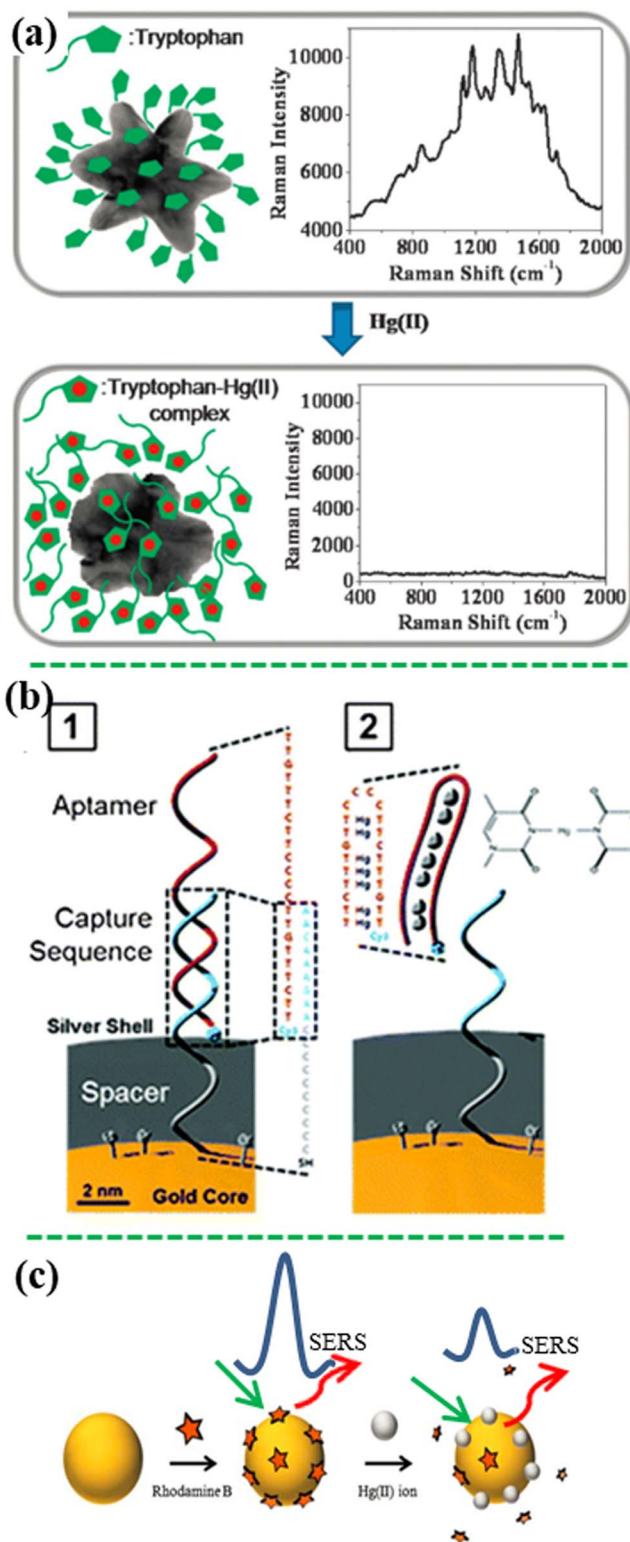


Figure 8. Detection of heavy metal ions by the “turn-off” strategies with use of SERS probes. Detachment of the SERS probes away from the plasmonic nanostructure, which is induced (a) by stronger binding with analyte metal ions,¹⁶⁶ or (b) by dissociation of DNA strands (modified by permission of Royal Society of Chemistry),¹⁷² or (c) by deactivating and competitive absorption (modified by permission of Springer-Verlag).¹⁷⁷

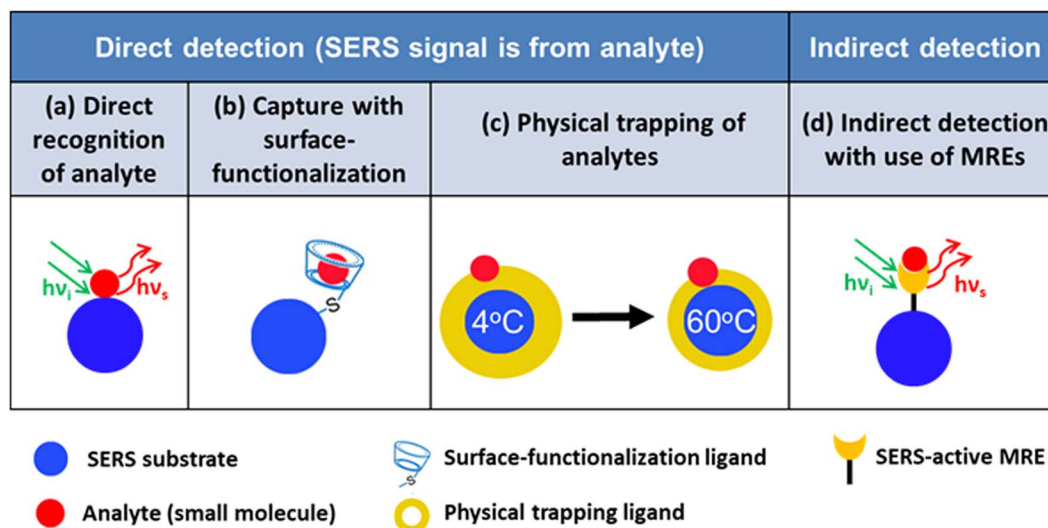


Figure 9. Illustration of different capture approaches for trapping small molecule during SERS detection. (a) Direct recognition of analyte with SERS spectra; (b) capture of analytes with the surface-functionalized SERS substrates; (c) physical trapping of analytes in proximity to the SERS substrate; (d) indirect detection with use of SERS-active MRE.

and used all over the world through the 1930's to 1980's as cooling/isolation fluids in closed systems like transformer and vacuum pumps, and also as fire retardants for electric/electronic equipment.¹⁸⁸ They can cause a variety of adverse health effects on immune system, reproductive system, nervous system and endocrine system.¹⁸⁹ It is difficult to degrade PCBs in the environment and organism, resulting in a worldwide distribution and persistent harms. Pesticides are used to prevent, destroy, repel, or mitigate a pest, or is plant regulators, defoliants, desiccants, or nitrogen stabilizers.¹⁹⁰ More than 1000 pesticides are widely used in modern agriculture. Pesticides can exist in farm products and be partly released into the environment, which in turn results in human exposure through intake of pesticide residues in food and drinking water.¹⁹¹ To make food delicious, look better, or be preserved for a longer time, some illegal or excess additives are added into food. For example, in September 2008, tens of thousands of infants in China were hospitalized, and several of them even died due to the intake of melamine in infant milk powder.¹⁹² Therefore, EPA has enacted a maximum residue limit for toxic small molecules in drinking water, such as 5 ppb for benzene, 0.2 ppb for benzo(a)pyrene, 0.5 ppb for PCBs, 40 ppb for carbofuran, 2 ppb for chlordane, 70 ppb for 2,4-Dichlorophenoxyacetic acid (2,4-D), and 0.2 ppm for dalapon, respectively.¹²¹

Sensor design.—Figure 9 schematically illustrates the design strategies of SERS sensors for detection of small molecules. Some of small molecules, especially dyes and aromatic molecules, have relatively large polarizability, which could generate considerable SERS signal. If such small molecules have some special functional groups such as thiols, amines and cyanides, they can be adsorbed firmly on the plasmonic metal surface through these chemical bonds. Hence, these molecules are easily excited to generate the characteristic SERS bands and measured directly with these SERS bands. However, if the small molecules cannot be adsorbed onto the plasmonic surfaces, for example, when the nonpolar organic pollutants meet a hydrophilic SERS substrate (Au and Ag), they cannot be directly captured by the bare plasmonic metal nanostructures. Hence the plasmonic metal surface has to be functionalized.

Direct recognition of analyte with SERS spectra.—If a small molecule analyte is SERS-active, and tends to be adsorbed chemically or physically on the surface of a plasmonic metal nanostructure, it can be directly detected using various SERS substrates. The target analytes are identified by the characteristic SERS vibration bands and quantified by the band intensity.¹⁹³ For example, Meng et al. have prepared

a self-assembled monolayer of silver nanocubes (Ag-NCs) on a flexible transparent polyethylene (PE) film, achieving a flexible SERS substrate (Figure 10a).⁶⁴ The “hot spots” both at the sharp corners of individual NCs and between the neighboring Ag-NCs contributed to highly sensitive detection of thiram adsorbed on silver surface through the Ag-S band. The flexible SERS substrate was employed to detect 10 nM methyl parathion in an orange by directly placing the SERS substrate on the orange peel, which demonstrated a great potential in practical food safety application. In addition, food additive such as melamine has been directly detected by the Ag-NPs decorated basil seeds^{194,195} and the gold nanofinger chips at a LOD as low as 120 ppt in water or 100 ppb in milk.¹⁹⁶ SERS substrates are the key to the success of SERS sensors. It is desirable to create high density of “hot spots” in a large area through ordered nano-array patterns. Figure 10b shows a large-scale flexible film of Ag-NPs decorated polyacrylonitrile (PAN) nanohump array pattern, which was able to detect methyl parathion (the pesticide residual) by swabbing the peel of apples.¹⁹⁷ Recently the ordered porous anodic aluminum oxide (AAO) membranes and the polystyrene sphere assemblies were used as templates to create highly ordered three-dimensional (3D) silver nanorod (NR) array^{74,77} and the Ag-NR bundle array (Figure 10c).⁸⁵ The 3D hierarchical structure not only generates more “hot spots” without increasing the footprint, but also creates stronger localized EM field. For example, “hot spots” were generated due to strong EM field coupling among the narrow gaps (2 nm) between the neighboring Ag-NRs at the top ends, as shown in Figure 10c. The Ag-NR bundle array showed SERS enhancement of 10^8 with good uniformity and high reproducibility (RSD < 10%). This SERS substrate was employed to detect multiple trace organic pollutants (methyl parathion and 2,4-D) simultaneously. Meng's group have also developed the Ag nanohemisphere array,^{75,76,83} the silver nanosheet-assembled cubes array,⁷⁰ and the silver dendrite clusters on the patterned sites⁹⁰ for direct detection of pesticides and plasticizers. Antibiotics like potassium benzylpenicillin was measured with the self-assembled silver colloid film.¹⁹⁸ Moreover, three antibiotics including chloramphenicol, ciprofloxacin and enrofloxacin have been detected with the silver dendritic substrate at a LOD on the nM order.¹⁹⁹

To enable direct detection by SERS substrates, analytes must be close to the SERS substrates through chemical binding or physical absorption like via Van der Waals' force. However, it is challenging to capture high nonpolar and hydrophobic molecules such as PCBs with SERS substrates. It is noted that the water solubility decreases with increasing the degree of chlorination in PCBs. Consequently only

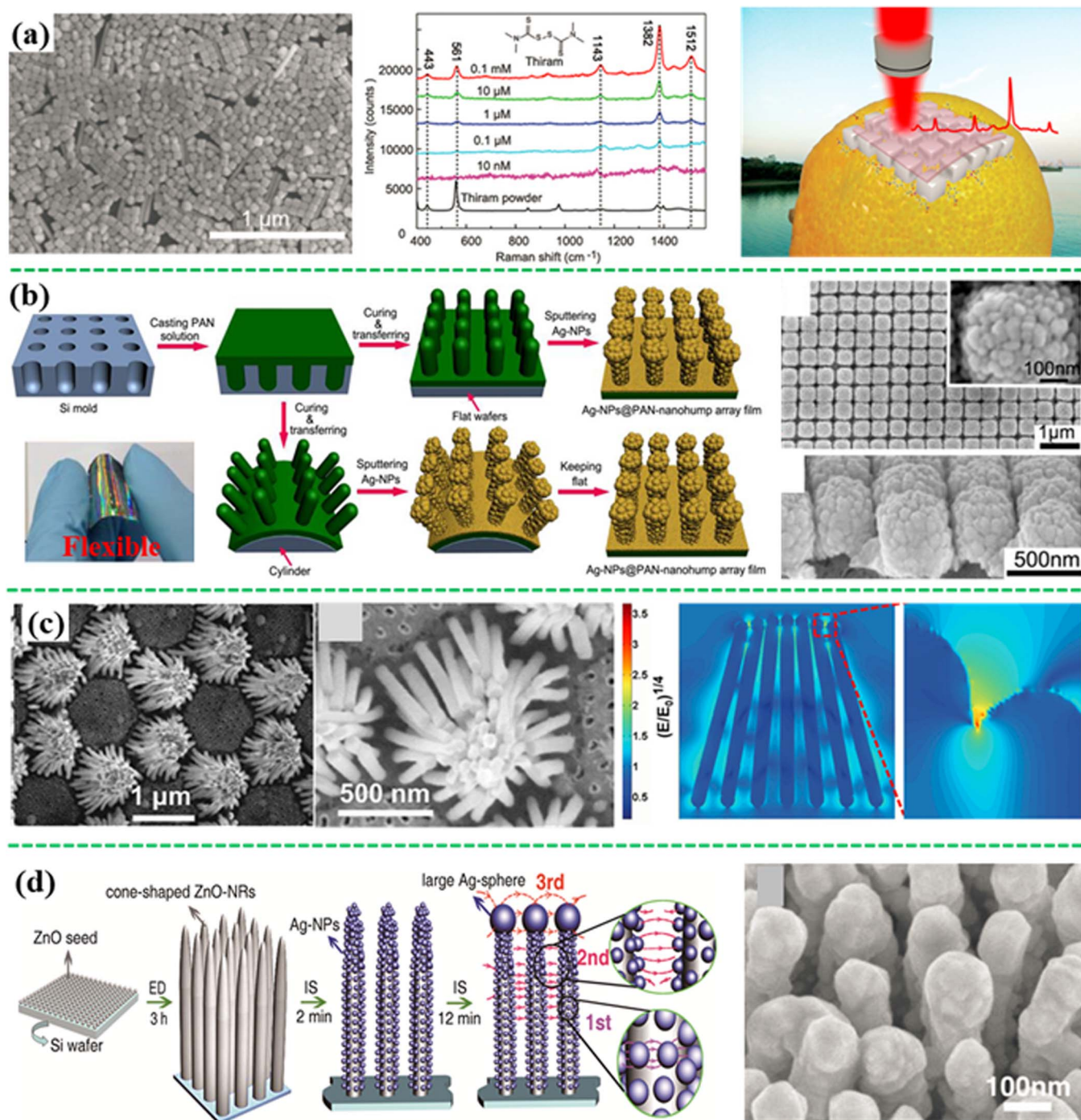


Figure 10. Various SERS substrates for direct detection of small molecules. (a) Self-assembled monolayer of Ag-NCs on a flexible transparent polymer film for detection of thiram, PCB-3 and methyl parathion on contaminated oranges (modified by permission of The Royal Society of Chemistry).⁶⁴ (b) A Large-scale flexible Ag-NP@PAN-nanohump array;¹⁹⁷ (c) a hierarchically ordered array of Ag nanorod bundle array with “hot spots” between the neighboring Ag nanorods;⁸⁵ (d) 3D SERS substrate of cone-shaped ZnO nanorods decorated with Ag-NPs (modified by permission of Wiley-VCH).²⁰⁰

high concentration of PCBs (higher than 1 μM) can be directly detected, especially for those with high degree of chlorination.^{64,75,76,197} However, low LODs have been reported in some cases. For example, 100 pM or 10 pM of PCB77 (3,3',4,4'-tetrachlorobiphenyl) was determined by the silver dendritic nanostructure film and the 3D hybrid SERS substrate of ZnO nanorods and Ag-NPs (Figure 10d), respectively.^{200,201} The close-packed 3D structures probably trapped the PCB molecules in the structure for direct detection. However, it's necessary to mention that, for the 3D Ag-NPs/ZnO nanorod hybrid substrate, photocatalytic degradation of PCB77 may happen based on

the previous research.²⁰² Intermediate products, which have similar chemical structures but higher affinity to the SERS substrate, could cause interference.

Capture of analytes with surface-functionalized SERS substrates.—When analytes cannot be directly absorbed on a bare SERS substrate, surface functionalization is performed on the SERS substrate surface. For example, hydrophobic organic molecules are used to modify the surface of SERS substrates to adsorb more nonpolar organic pollutants that have very low affinity to SERS substrates, like PAHs and PCBs. Graphene or molecules with benzene ring could also improve

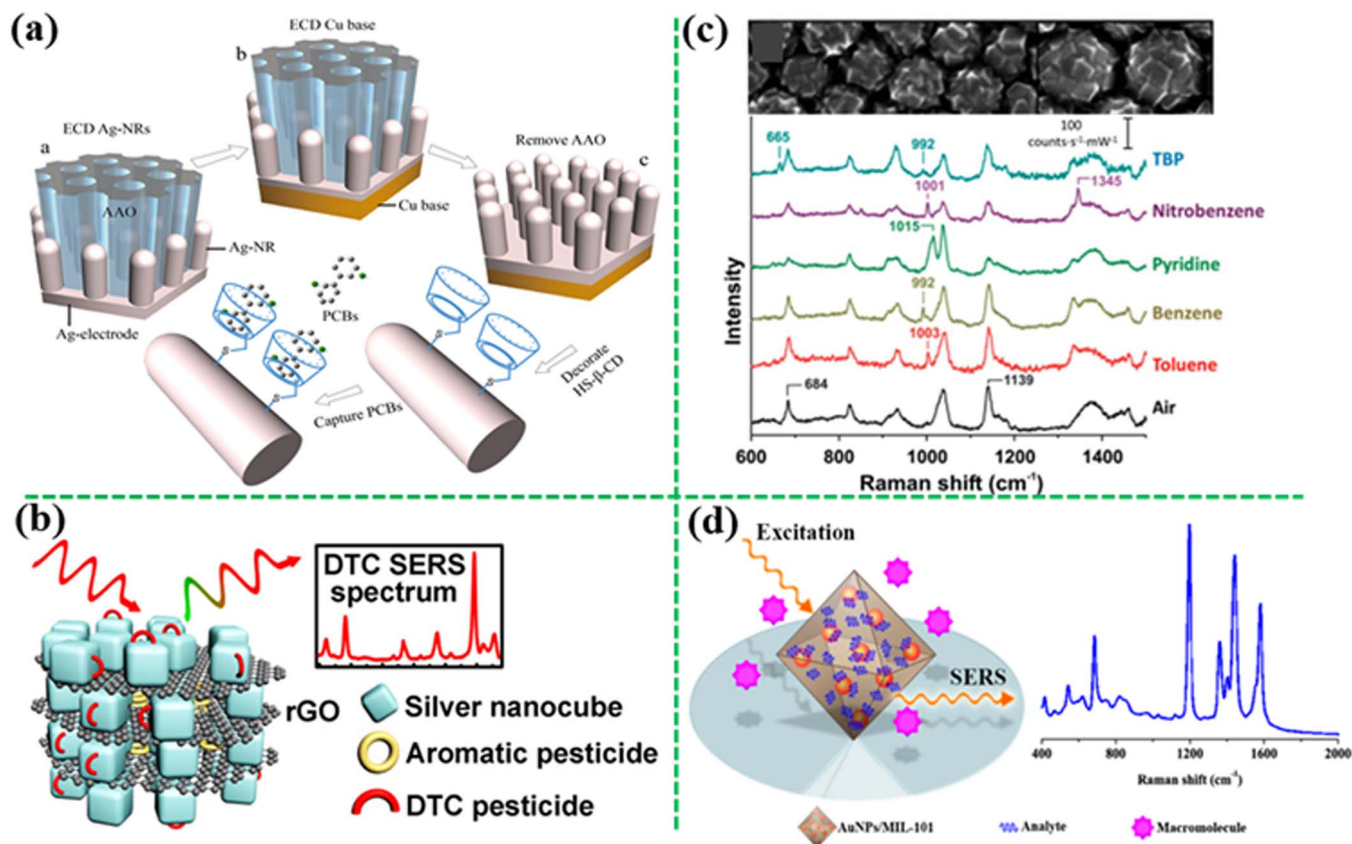


Figure 11. SERS sensors with surface-functionalized substrates for capture of analytes. (a) Cyclodextrin-modified Ag nanorods for capture of PCBs (modified by permission of John Wiley & Sons).⁷⁷ (b) The rGO-wrapped Ag nanocubes showing high affinity to aromatic pesticides (modified by permission of American Chemical Society).²¹⁰ (c) the MOF-functionalized-Ag film on sphere array (d) or the MOF filled with the Au-NPs showing high SERS sensitivity to molecules that do not adsorb on metal surface (modified by permission of The Royal Society of Chemistry and American Chemical Society, respectively).^{211,212}

the affinity of SERS substrate to the analytes because of the π - π interactions. Alternatively, the materials that have high adsorption capability such as metal-organic framework (MOF) are incorporated with SERS substrates to enhance analyte capture.

Haynes et al. have successfully detected PCB47 (2,2',4,4'-tetrachlorobiphenyl) and PCB77 using the decanethiol-modified silver film on a silica nanosphere array based on the hydrophobic interactions between PCBs and decanethiol, achieving a LOD of 50 pM.^{203,204} Decanethiol was also decorated on a vertically aligned Ag nanoplate-assembled film, achieving a low LOD of 100 nM for PCB77.⁷¹ A sol-gel film encapsulated Ag-NPs functionalized with 25,27-dimercaptoacetic acid-26,28-dihydroxy-4-tert-butylcalix[4]arene (DMCX) was synthesized in situ for detection of PAHs in seawater at a LOD of 0.3 nM for pyrene and 13 nM for naphthalene due to the formation of the host-guest complex with DMCX.²⁰⁵ It has been reported that cyclodextrin had a hydrophobic inner surface, which could capture the guest molecules PCBs to form stable host-guest inclusion complexes, and thus effectively trap and detect PCBs.²⁰⁶⁻²⁰⁹ Thio-cyclodextrins were also decorated on the large-scale well-separated Ag nanosheet-assembled micro-hemispheres and Ag nanorods array (Figure 11a), which can create a large number of "hot spots" at the small gaps between the neighboring Ag nanosheets or Ag nanorods, showing high sensitivity toward PCBs, that is, 300 nM PCB77, 10 nM PCB1 (2-chlorobiphenyl), 20 μ M PCB29 (2,4,5-trichlorobiphenyl) and 20 μ M PCB101 (2,2',4,5,5'-pentachlorobiphenyl).^{72,73,77} Meng et al. have developed a sponge-like SERS substrate made of the rGO-wrapped Ag NCs for selectively detecting dithiocarbamate pesticides from aromatic pesticides, such as methyl parathion, DDT, isazofos, thiophanate-methyl, and carben-dazim, which were adsorbed on rGO via the π - π interaction between

the rGO and the aromatic rings (Figure 11b).²¹⁰ The hybrid structure of MOF and plasmonic structure, either through decorating MOF on the plasmonic structure surface (Figure 11c) or imbedding the plasmonic nanoparticles in the MOF matrix (Figure 11d), were used to trap and subsequently detect a range of similar volatile organic compounds such as benzene, toluene, nitrobenzene, 2,6-di-tert-butylpyridine, benzadine, p-phenylenediamine and tumor marker alpha-fetoprotein in human serum using the high adsorption capability of MOF.^{211,212}

Physical trapping of analytes close to SERS substrates.—Physical trapping is another strategy to capture analytes to the SERS substrate surface. For polar or charged analytes, electrostatic attraction can be used to concentrate the analytes on the SERS substrates. Polar analytes can be selectively attracted to an oppositely charged electrode applied with a small potential (electrostatic preconcentration), lowering the LOD accordingly.²¹³⁻²¹⁵ For example, polar antibiotics, such as 6-aminopenicillanic acid and penicillin G, were selectively concentrated and detected on the surface of Ag-NPs grafted germanium nanowires on a copper grid by changing applied potential, showing a LOD of 2.4 nM and 0.9 nM, respectively (Figure 12a).²¹³ Similarly, aniline and phenol derivatives can be selectively adsorbed from a mixture of polar pollutants on the silver-electrodeposited screen-printed electrodes by controlling the polarity of the applied potential.²¹⁴

Moreover, mechanical force can also be used to confine the analytes close to a SERS substrate to enhance the SERS signal. For example, if the SERS substrates are coated with the temperature- or humidity-sensitive materials, change in temperature or humidity will trigger the shrink or expansion, reducing the space between the SERS substrate and the analytes, enhancing the SERS signal. For example, the Au-NPs coated with a thermally responsive poly-(N-isopropylacrylamide) (pNIPAM) microgel can trap the analytes.

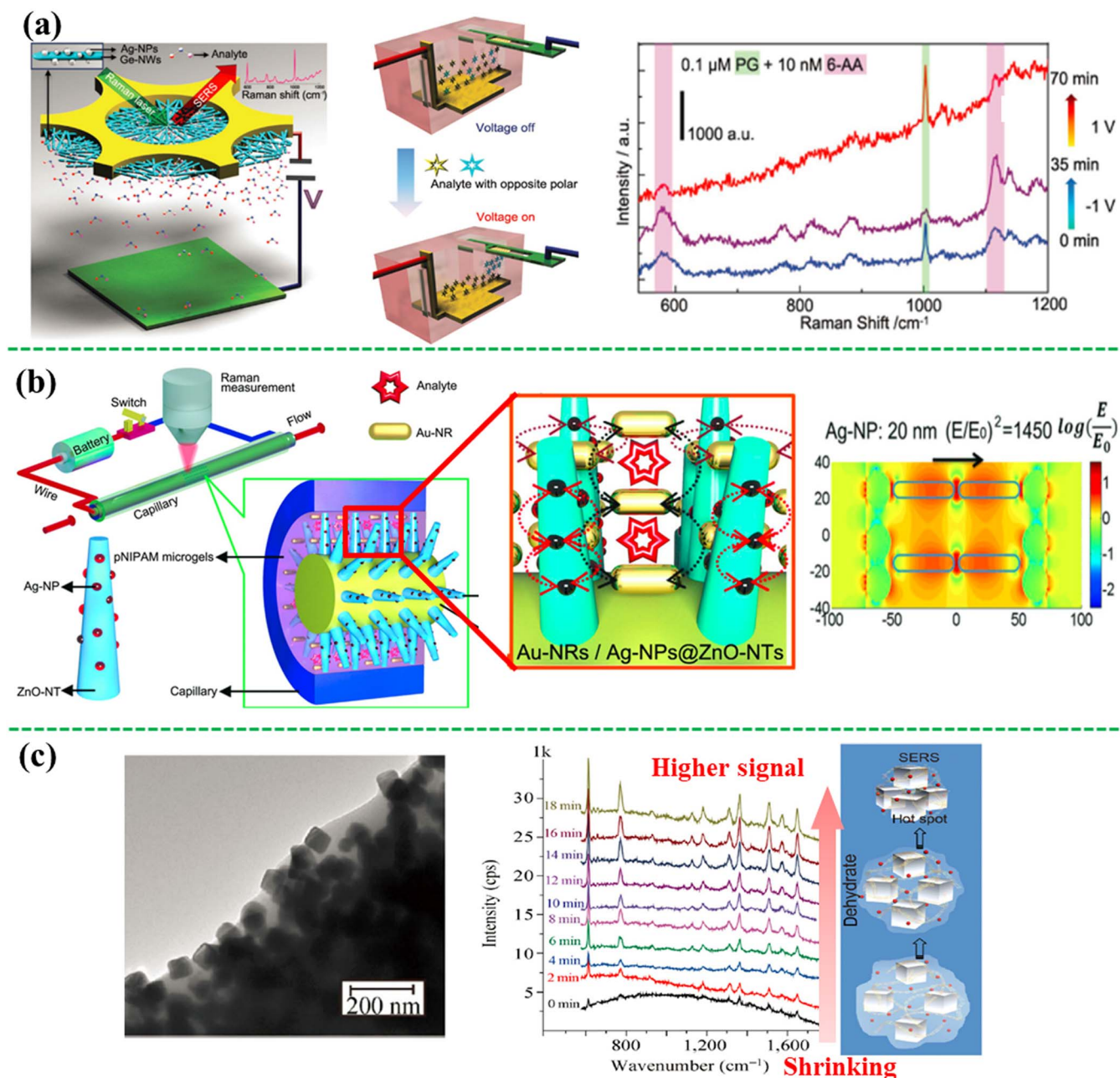


Figure 12. SERS sensors through physical trapping of analytes. (a) Electrostatic preconcentration of polar molecules using the Ag-NP-grafted germanium nanowires on a copper grid, showing selective detection of opposite polar molecules by changing potential polarity (modified by permission of Wiley-VCH).²¹⁵ (b) A compact electrical heating-controlled SERS fluidic system based on Au-nanorods/Ag-NPs@ZnO-nanotaper@Cu wire (modified by permission of the authors and the institute).²¹⁷ (c) A humidity-sensitive Ag-NCs@PAAS network, trapping the analytes in the small gaps among the Ag-NCs during dehydration-induced shrinking (modified by permission of Tsinghua University Press and Springer).²¹⁸

When it is heated up, pNIPAM will shrink and carry the analyte molecules toward the plasmonic Au NPs.²¹⁶ Following this mechanism, the thermo-responsive microgel was used in a compact electrical heating-controlled SERS fluidic system for capture and detection of trace small molecule pollutants such as 100 nM methyl parathion in water (Figure 12b).²¹⁷ A constantan wire covered with the ZnO nanotapers decorated with Ag-NPs was inserted into a glass capillary filled with a mixture of the pNIPAM microgels and the Au-nanorod colloids. After the analyte solution was filled into the capillary, the system was heated by applying a potential on the constantan wire. As a result, the pNIPAM microgels shrank, immobilizing the analyte and driving the Au-nanorod close to both each other and the Ag-ZnO nanotapers. This created high-density of “hot spots” due to multi-type plasmonic

couplings in a 3D space, amplifying the SERS signal. Additionally, the humidity-sensitive materials were used to capture analytes. Meng et al. have developed a networked polyacrylic acid sodium salt (PAAS) film entrapped silver-nanocubes (Ag-NCs@PAAS) to physically confine the analytes at the surface of Ag-NCs (Figure 12c).²¹⁸ In the presence of analyte solution, the dry Ag-NCs@PAAS substrate would swell because of the bibulous PAAS, pushing away the neighboring Ag-NCs. Consequently the analytes diffused into the interspace among the neighboring Ag-NCs. After drying, the PAAS shrank and pulled the Ag-NCs back to the aggregated state with the analytes in the small gaps between the Ag-NCs, inducing the “hot spots” and strong SERS signal. Using this substrate, melamine, adenine, methyl parathion, glucose molecules and their mixture have been sensitively detected.

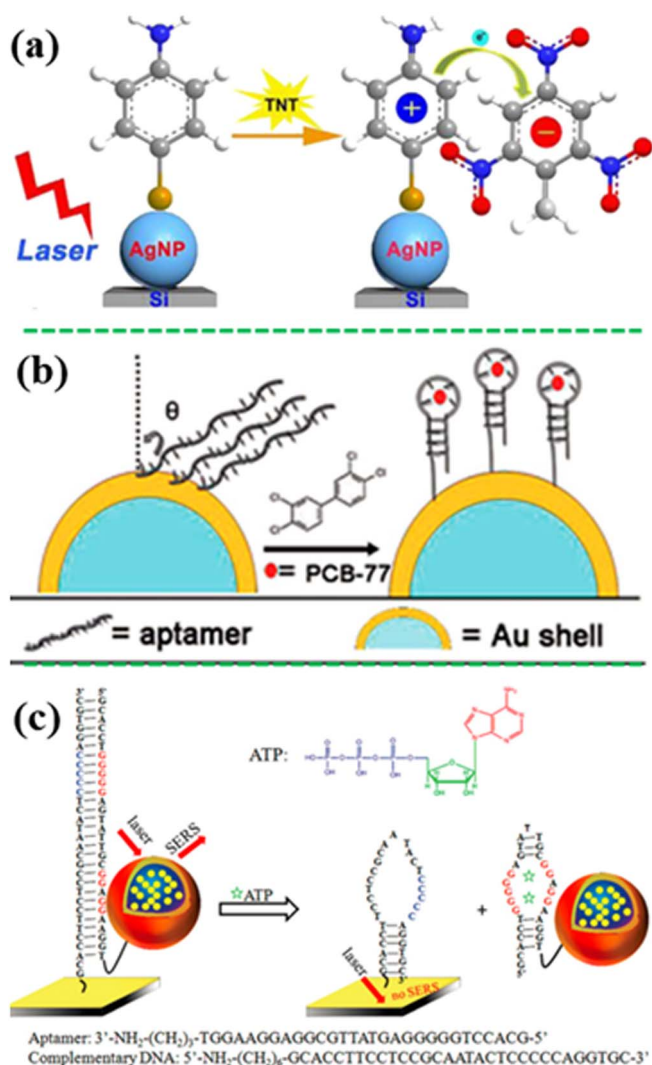


Figure 13. Indirect detection of small molecules with assistance of MREs. (a) The presence of TNT turned on SERS activity of 4-ATP-decorated Ag-NPs on silicon wafer due to the formation of TNT–4-ATP complex (modified by permission of American Chemical Society).²²¹ (b) Detection of PCB77 with an SERS-active aptamer MRE (modified by permission of The Royal Society of Chemistry).²²³ (c) Detection of ATP using the SERS probe-linked aptamer (modified by permission of American Chemical Society).²²⁴

Indirect detection with use of MREs.—To detect small molecule analytes with low polarizability, MREs are used to selectively capture the targets. TNT (2,4,6-Trinitrotoluene) is not easily detected directly due to its low polarizability and poor affinity to plasmonic Au or Ag nanostructures. Therefore, SERS-active 4-ATP was used as a MRE to capture it.^{197,219–221} For example, Chen et al. developed a 4-ATP-modified Ag NP-silicon wafer (AgNP@Si) substrate for TNT detection (Figure 13a).²²¹ When TNT was present in the assay, the TNT–4-ATP complex was formed, transforming 4-ATP from a nonresonant state to an electronic state, and lighting up SERS signals of 4-ATP. As a result, this sensor showed a linear range from 10 pM to 100 nM with the RSD of less than 15% and a LOD of 1 pM, 5 orders of magnitude lower than the MCL value suggested by EPA. Figure 13b revealed an aptamer-modified SiO₂@Au core/shell nanoparticles, in which the aptamer selectively bound to PCB77. As a result, the intensity ratio of bands 656 cm⁻¹ and 733 cm⁻¹ in the aptamer changed with variation of the PCB77 concentration, enabling quantitative measurement of 1 μM PCB77.^{222,223} In addition, Wu et al. have developed an aptamer-based SERS sensor for detection of adenosine triphosphate (ATP).²²⁴ The SERS probe-linked DNA was covalently bound to the

Table I. NIAID-categorized pathogen and examples.²²⁵

Category	Pathogens examples
A: Highest risk to national security and public health	-Bacillus anthracis -Clostridium botulinum toxin (botulism) -Yersinia pestis (plague) -Variola major (smallpox) & related pox viruses
B: Second highest priority	-Francisella tularensis -Viral hemorrhagic fevers -Diarrheagenic E.coli -Pathogenic Vibrios -Shigella species -Salmonella -Caliciviruses -Hepatitis A -Microsporidia
C: Third highest priority and include emerging pathogens	-Nipah and Hendra viruses -Additional hantaviruses -Tickborne hemorrhagic fever viruses -Tickborne encephalitis complex flaviviruses -Yellow fever virus

Au chip (Figure 13c), in which the SERS probes (the sandwiched Au nanostar@MGITC@SiO₂ NPs) were brought in proximity with the Au chip. Strong SERS signal can be detected from such an ensemble. When the ATP molecules were present in the SERS assay, two ATP molecules were intercalated into each aptamer by forming the non-canonical G/A base pairs, leading to the dissociation of the duplex DNA. Consequently, the SERS probes were detached from gold film surface, reducing the SERS signal, achieving a LOD of 12.4 pM for ATP.

Detection of pathogens.—Motivation.—The pathogens are classified into three categories by U.S. National Institute of Allergy and Infectious Disease (NIAID) as shown in Table I.²²⁵ Pathogens including bacteria, virus and fungi, which are present in food and environment, pose high risk of health hazards worldwide. They can be reproduced rapidly and disseminated through air, water and food chain. Food-borne illness outbreaks happen worldwide. The Center for Disease Control and Prevention (CDC) has estimated that about 1 in 6 Americans (48 million) get sick; 128,000 are hospitalized; and 3,000 died from food-borne disease each year.²²⁶ In U.S., 714 people got sick and 9 died in a *Salmonella* outbreak for peanut butter in 2009; and 907 people were ill and 1 died for the imported Mexican cucumbers in 2015.²²⁷ Consequently, the demand for rapid, accurate, sensitive, selective detection of food- and water-borne pathogens is continuously rising for public health.

Sensor design.—Fingerprinting SERS spectra of some pathogens could be obtained because of the presence of specific nucleic acid, amino acid, proteins, polysaccharides, carbohydrates and lipids. The SERS spectra obtained may be analyzed statistically via the pattern recognition. Besides direct recognition with SERS spectra, pathogens are also captured and recognized by MREs, and detected with assistance of SERS probes.

Direct recognition of analyte with SERS spectra.—Compared with inorganic ions and small organic molecules, pathogens have much larger size and more complicated chemical components, including proteins, nucleic acid, enzymes, and various inorganic and organic agents. Although SERS spectra have fingerprint feature, the complicated spectra of pathogens make it not straightforward to identify the specific target in some cases. And there is no any complete SERS spectrum database for pathogens.²⁷ Therefore, chemometrics is used to assist the qualitative and quantitative analysis of the SERS spectra obtained. Multivariate data analysis are the commonly used statisti-

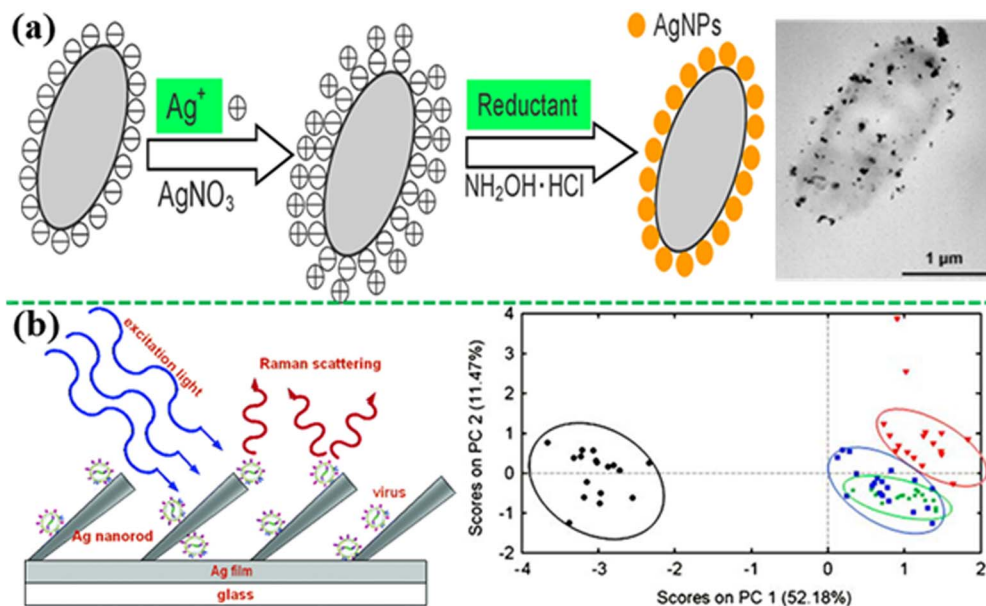


Figure 14. (a) In-situ growth of Ag NPs on the bacterial surface for direct SERS sensing (modified by permission of American Chemical Society).²³⁵ (b) Direct detection of virus using a silver nanorod array and the subsequent PCA analysis of the SERS spectra of four virus strains (modified by permission of American Chemical Society).²³⁷

cal approach,^{25,159} including principal component analysis (PCA) and partial least squares (PLS) regression.

Generally, there are three different strategies for SERS sensing of pathogens: (i) placing the whole pathogens cells directly on a solid SERS substrate; (ii) mixing pathogens with plasmonic metal NPs in a solution to induce aggregation or a sandwich structure; and (iii) assembling plasmonic metal NPs directly onto the surface of pathogens.

Biomarkers from *Bacillus*, such as calcium dipicolinate (CaDPA) or dipicolinic acid (DPA) in bacterial spores, can be used for direct SERS detection of *Bacillus*.²²⁸ The SERS peak at $\sim 1001\text{ cm}^{-1}$ assigned to the ring breathing vibration was used for DPA quantification. Van Duyne et al. have used a silver film over the polystyrene nanosphere substrates to detect the CaDPA in *anthrax* spores, achieving a LOD of 2.6×10^3 spores.^{229,230} Silver colloids were also used to detect and quantify the DPA biomarker in *Bacillus* spores at a level of 5 ppb (29.9 nM).²³¹

In some cases, SERS spectra obtained from the cell wall (nucleic acids, proteins, polysaccharides, carbohydrates, and lipids) were used for direct recognition.^{232–234} For example, the bacterium *Geobacter sulfurreducens* was detected by the in vivo reduced Au^{3+} within the cytoplasm close to the inner cell membrane, and recognized by the SERS band at 1250 cm^{-1} , which was associated with proteins in cell membrane and cytosolic proteins.²³² In addition, Haisch et al. deposited Ag NPs directly on the cell wall of bacteria to detect the living bacteria in drinking water (Figure 14a).²³⁵ They found that the SERS enhancement with in-situ growth of Ag NPs on the bacteria surface was about 30 folds higher than that in the case of a simply mixed colloid–bacterial suspension. Three strains of *Escherichia coli* and one strain of *Staphylococcus epidermidis* were discriminated by hierarchy cluster analysis, achieving a LOD of 250 cells/mL after SERS mapping.

Viruses could also be directly detected via their characteristic SERS vibration bands. For example, various viruses such as norovirus, adenovirus, parvovirus, rotavirus, coronavirus, paramyxovirus and herpesvirus, have been discriminated with the gold nanostructures.^{236,237} Moreover, Tripp et al. have used a silver nanorod array to directly detect human respiratory viruses (Figure 14b). The SERS bands at 527 cm^{-1} and 546 cm^{-1} could be assigned to a disulfide stretching mode for respiratory syncytial virus. Multivariate statisti-

cal analyses, including soft independent modeling of class analogy (SIMCA) and PCA, were employed to effectively discriminate three types of wild strains of respiratory viruses and the DNA sequences with a single gene mutation.²³⁸

Indirect detection with use of MREs.—Whole pathogens can be indirectly detected by combining the SERS probes with MREs such as antibodies, aptamers and small molecule ligand (e.g. glutaraldehyde, and 3-mercaptophenylboronic acid). For example, on-line screening of *Salmonella Choleraesuis* and *Neisseria lactamica* have been realized with integration of nanoaggregate-embedded beads SERS probes and microfluidic device (Figure 15a).²³⁹ The probes were silica-coated dye-induced aggregates of a small number of Au NPs, immobilized with specific antibody on the bead surface as the MRE. Strong signal can be created owing to the presence of “hot spots” at junctions between Au NPs, showing a detection capability down to a single bacterium (70 CFU/mL). Compared with ELISA, this SERS sensing strategy provided higher sensitivity and required lower amount of antibody. *Salmonella typhimurium* was detected with a spiny Au NP-based SERS sensor.²⁴⁰ The spiny Au NP were functionalized with 4-MBA as the SERS probe, and linked to a thiolated aptamer as the MRE for the capture of *S. typhimurium*. This sensor showed a dynamic detection range from 10 CFU/mL to 10^5 CFU/mL at a LOD of 4 CFU/mL. Similarly, using two different specific bonding aptamers, *S. typhimurium* and *S. aureus* were detected simultaneously at a LOD of 15 CFU/mL and 35 CFU/mL, respectively.²⁴¹ In addition, viral zoonotic pathogens, *West Nile virus* and *Rift Valley fever virus* were detected by the Au NPs coated with the SERS probes and the specific antibody.²⁴² It showed a LOD of 5 fg/mL in a phosphate buffered saline buffer (PBS) and 25 pg/mL in a PBS spiked fetal bovine serum. Similarly, other antibodies or small-molecule ligands (e.g. glutaraldehyde,²⁴³ and 3-mercaptophenylboronic acid) have also been used as the MREs for SERS detection of other bacteria such as *E. coli*, *Salmonella typhimurium* DT10.^{244–247}

Besides using MREs for the recognition of whole pathogen, SERS sensor can identify pathogen through detecting the characteristic DNA extracted from pathogens. Recently, hepatitis B virus (HBV) DNA was successfully detected with a SERS sensor based on the typical sandwich configuration (Figure 15b).²⁴⁸ A single-stranded capture DNA complementary to the HBV DNA was immobilized on a periodic Au triangle nanoarray pattern. The assay also contained the detection

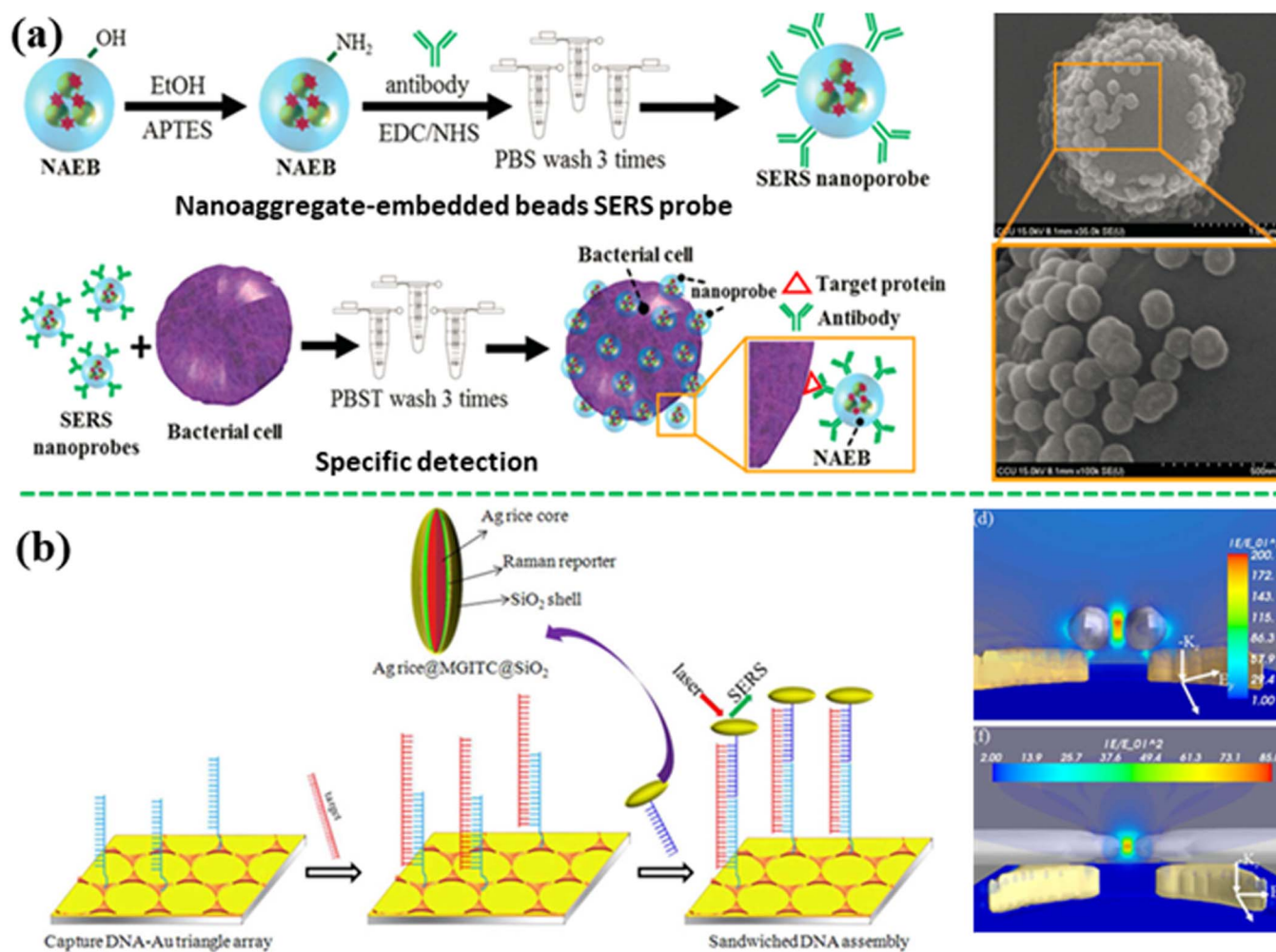


Figure 15. (a) Indirect detection of *Salmonella Choleraesuis* and *Neisseria lactamica* with the antibody-functionalized nanoaggregate-embedded beads SERS probe (modified by permission of Wiley-VCH).²³⁹ (b) Indirect detection of hepatitis B virus DNA using a sandwich-structured SERS sensor by coupling the SERS probes onto a gold triangle array pattern (modified by permission of American Chemical Society).²⁴⁸

DNA linked to a SERS probe (the sandwiched Ag nanorice@Raman label@SiO₂ NP). When the HBV DNA appeared in the assay, the HBV DNA was hybridized with both the capture and the detection DNA strands, which made the SERS probe coupled to the periodic Au triangle nanoarray pattern, generating the “hot spots” in the 3D space. As a result, such a sensor achieved a LOD of 50 aM for HBV DNA.

Integration of SERS Sensors into Microfluidic Chips

Previous review papers have dealt with microfluidic platforms,^{249–252} and paper-based lateral flow strip.^{253–258} Herein this article just highlights the SERS sensors integrated into microfluidic chips. The combination of SERS with microfluidics also refers as lab-on-chip SERS, or optofluidic SERS devices, which realize sample-pretreatment, detection and flow control with a single microfluidic chip. This enables automation, miniaturization and portability for field-deployable applications. Generally, an active microfluidic system includes micropumps, microvalves, micromixers and detectors. SERS sensors have been integrated into two types of active microfluidic systems: the continuous flow platform and the segmented (or droplet) flow platform. The continuous SERS-microfluidic systems are capable of highly reproducible measurement and effectively dissipation of heat, which benefits to photosensitive or heat-sensitive analytes. However, the analytes may sometimes get enriched over time on channel walls, leading to the memory

effect. And the molecular diffusion induced mixing in the continuous flow microfluidics is relatively slow with the typical microfluidic channel width. In contrast, the segmented flow microfluidic devices avoid mixing between two miscible liquid streams by introducing a gas phase or oil phase.^{172,259,260} The segmented flow platforms can separate the continuous sample flow and colloidal nanoparticles by droplets of an immiscible fluid phase. The memory effect can be reduced because the droplets avoid significant liquid exchange between the liquid segments.

Figure 16a shows a continuous flow SERS device integrated with the Ag NPs functionalized with GSH (MRE) and 4-MPY (SERS probe).²⁶¹ When the As³⁺ ions and the functionalized Ag NPs are introduced into the microfluidic channel, the As³⁺ ions bound to GSH, leading to the aggregation of functionalized Ag NPs. This resulted in the “hot spots” between the adjacent Ag NPs, amplifying the SERS signals of 4-MPY. Such an optofluidic SERS device exhibited a linear range from 3 to 200 ppb at a LOD of 0.67 ppb. Figure 16b shows a droplet microfluidic device for detection of Hg²⁺ ions in water, achieving a LOD of 10 pM.¹⁷² The aptamer-linked SERS probes were immobilized on the surface of Au-Ag core-shell NPs via hybridization of a complementary DNA covalently linked to the NP. Small water droplets containing the Hg²⁺ ions were separated from each other by an oil phase, which flowed along the microfluidic channel. When Hg²⁺ ions bound to the aptamer, a hairpin structure was formed, leading to detachment of the SERS probe-linked aptamer away from the Au-Ag NPs. This tuned off the SERS signal.

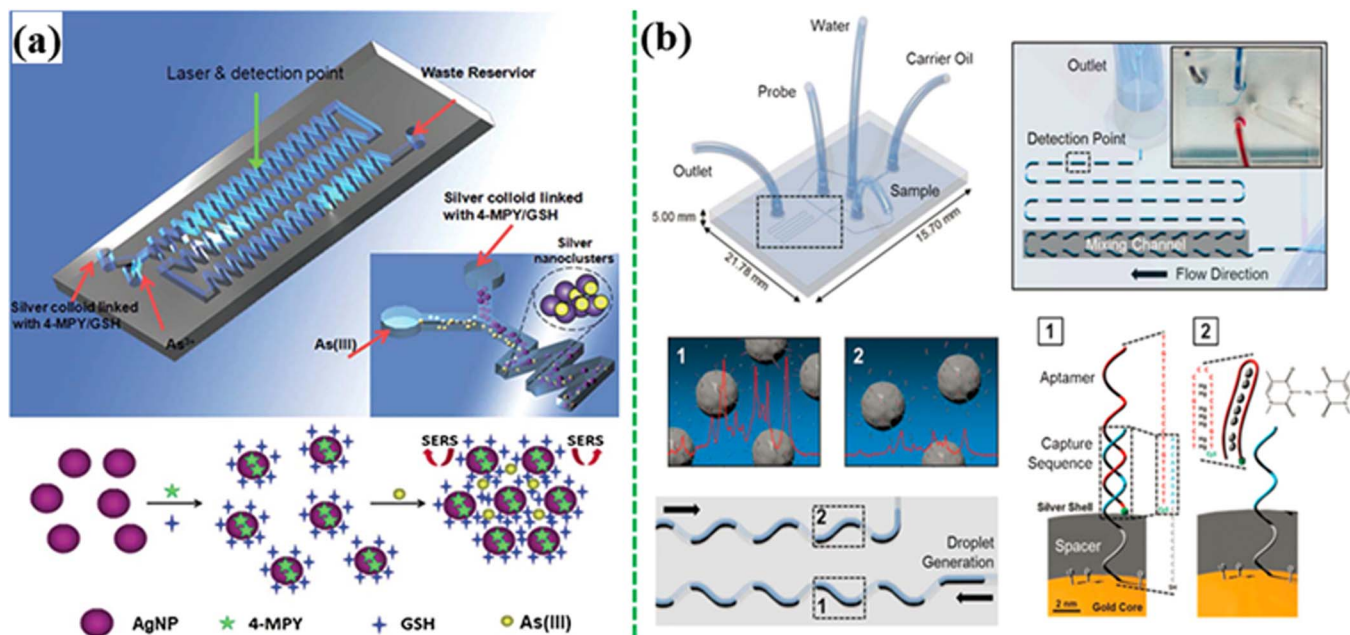


Figure 16. (a) A continuous flow microfluidic device for detection of As^{3+} with Ag-NPs conjugated GSH and 4-MPY (modified by permission of The Royal Society of Chemistry).²⁶¹ (b) A segmented flow microfluidic device for Hg^{2+} ion detection with aptamer-modified Au/Ag core-shell nanoparticles (modified by permission of The Royal Society of Chemistry).¹⁷²

Active microfluidic devices need microvalves and pumps for driving and controlling the flow, which increase the cost and have relatively large footprint for whole systems. Passive microfluidic devices such as lateral flow strips utilize the capillary forces to drive and control the flow, which do not require the pumps and the associated control systems. In particular, paper-based lateral flow strips (PLFS) are inexpensive, user-friendly, and easy to operate. Therefore, integration of SERS sensors with PLFS arouses strong interest.²⁵⁸ A typical SERS PLFS consists of several porous carriers including a nitrocellulose membrane, a sample pad, a conjugate pad and an absorption pad (Figure 17).²⁵⁸ When the liquid sample is dropped onto the sample pad, liquid will flow through the conjugate pad by the capillary force. Meanwhile, the analyte binds with the SERS probes through the conjugated antibodies, forming complexes of target analyte-detection antibodies labeled SERS probes. Finally, the resulting complexes flow to the test line, and are captured by the capture antibody. As a result, the SERS probes are accumulated on the test line through the formation of sandwich structure. The excessive SERS probes, which are not immobilized on the test line, continue to diffuse and are captured by the other antibodies anchored on the control line. Consequently, two greyish bands are displayed on both the test line and the control line. A portable Raman spectrometer is employed to record the signal of SERS probes at the test line, which is correlated with the analyte concentration. So far, pathogens and heavy metals have been detected selectively.^{254,262}

Conclusions and Perspectives

Most of the papers on SERS sensors have been published since 2000s; and the number of relevant papers increased in 2010s, indicating expedited development and increasing applications of SERS sensors. In the last two decades, various plasmonic metal nanostructures have been developed as the SERS substrates to improve the sensitivity, repeatability and massive production of SERS sensors. Among various plasmonic Au, Ag, Cu and Al materials, Au is the most appealing to SERS sensors due to its high stability and reasonably strong plasmon. Ag has the strongest plasmon and is widely used in SERS research but the stability is of concern in some cases. Cu was not used because it was considered as weak plasmonic material. Recent studies

reveal that Cu nanocubes exhibit strong and narrow LSPR peak.^{263–266} Al typically shows the SPR peak in ultraviolet range.²⁶⁷ Hence it is not widely used either. Recently, plasmonic semiconductors such as WO_{3-x} , MoO_{3-x} , Cu_{2-x}S , with high charge carrier concentration by heavily doping also attracted interests in SERS,²⁶⁸ catalysis,²⁶⁹

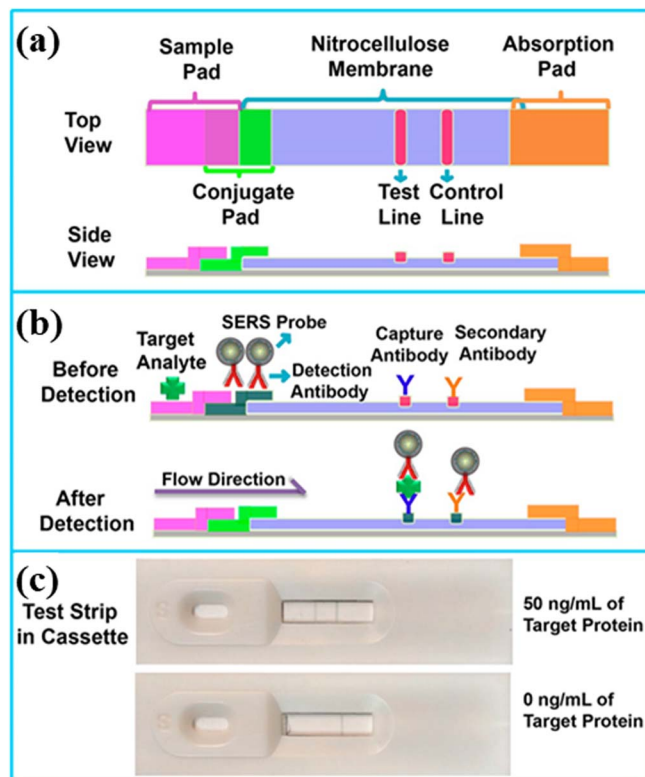


Figure 17. SERS paper-based lateral flow strip design and operation principle (modified by permission of American Chemical Society).²⁵⁸

and solar energy field.^{270,271} The shape of the plasmonic nanoparticle has the most effect on enhancement of localized EM field. Among nanospheres, nanorods, nanocubes, nanostrars, nanocages and other shapes, nanostars are the most attractive due to their strongly enhanced EM field, easy synthesis and tunable LSPR band at around 785 nm, which is in resonance with the popular near-infrared laser source. Chip-based SERS substrates become very popular for SERS sensors. In particular, large-area ordered nano-array patterns, which are fabricated with the massive production processes, are of particular to SERS sensors because of their tailorable plasmonic properties and better controllability and repeatability than the disordered patterns. In the nano-array patterns, “hot spots” are created not only surrounding individual nanostructures, but also in the narrow gaps (typically < 10 nm) between two neighboring nanostructures. Coupling of SERS probes (containing plasmonic NPs) onto a periodic nano-array pattern can increase the local EM field of “hot spots” and extend “hot spots” into a large space without increasing the footprint. By utilizing this configuration, Wu’s group has developed a SERS immunoassay,²⁷² which mimics the configuration of ELISA. This lab-on-chip style of SERS immunoassay can be directly applied to the real-world complex sample matrices such as urine, milk fruit juice and blood serum/plasma, and even shows higher sensitivity than ELISA.

Some of analytes can be identified with SERS spectra because the fingerprinting SERS bands can be obtained from these analytes. To distinguish SERS spectra with small difference, chemometric analysis such as the pattern recognition method is necessary to categorize and quantitatively analyze the SERS spectra. Currently the height of individual SERS peaks selected is typically used for building the calibration curve for quantification of analyte concentration. Alternatively, it is interesting to use the whole SERS spectra for quantification of analyte concentration by utilizing the statistical algorithms.

When analytes are SERS-inactive or not able to generate fingerprinting SERS bands, MREs and SERS probes are typically used in SERS sensors to recognize and transduce SERS signals. Organic Raman reporter molecules such as MBA and MGITC generally are not directly used as the SERS probes/labels in sensors because they have extremely low scattering cross section, generating very weak SERS signal. Instead, these Raman reporter molecules are typically conjugated with a plasmonic nanoparticle to obtain strong SERS signal. In particular, the sandwich-structured SERS probes (e.g., Au nanostar@MGITC@silica NPs) are of particular interest into SERS sensors because they are of characteristic of excellent water-solubility, strong SERS amplification capability and easy conjugation with MREs or bio-molecules.⁴⁶

The goal of sensor development is to realize the on-site or real-time detection in the field or in the point-of-care (POC) settings. Because SERS-based lab-on-chips are necessary for realizing automation, miniaturization and portability in many cases, more efforts are needed to develop optofluidic SERS devices. On the other hand, both the size and cost of Raman spectrometers have been reduced dramatically in the last two decades. Handheld spectrometers become commercially available. It is desirable to develop portable SERS detection systems that integrate the SERS sensors, the microfluidic modules, the miniaturized Raman spectrometer and the user-interface control together. For example, this kind of integrated SERS detection systems may look like a carry-out briefcase (or box).

Current smartphones are equipped with several components that can be interfaced with sensors, including camera, global positioning system (GPS), Bluetooth, computer and an open software development platform for adding applications. Therefore, integration of sensors with smartphones has been under rapid development in recent several years, which is shifting the paradigm of sensor development. Indeed a smartphone was integrated into a Raman microscope to enable the phone’s camera to capture Raman images.²⁷³

The development of smartphone and 3D printing technology significantly pushed POC devices toward low-cost, user-friendly, on-site and on-time diagnostics. A variety of PLFS, microfluidic platforms, and wearable sensors have been designed for such as metal

ions,²⁷⁴ glucose,²⁷⁵ and pathogens²⁵⁷ based on paper, plastic, or flexible polymers materials. Besides with SERS, POC devices utilizing fluorescence, colorimetry and electrochemistry have also been developed.^{15,26,276,277} Compared to these POC devices, SERS-based devices have advantages in specificity and resistance to interference because of the fingerprint effect. However, SERS sensors have some limitations. First, lenses are typically used in SERS readers, which require the accurate position of SERS substrate. Second, the size and cost of SERS readers need to be further reduced toward wide applications in the POC settings.

Acknowledgments

We appreciate the financial support from NSF (CBET-1336205) and Natural Science Foundation of China (51628202 and 51632009), the CAS/SAFEA International Partnership Program for Creative Research Teams, as well as the Key Research Program of Frontier Sciences, CAS (QYZDJ-SSW-SLH046). H.T. is grateful to the support from China Scholarship Council.

ORCID

Nianqiang Wu  <https://orcid.org/0000-0002-8888-2444>

References

1. T. Zheng, T. R. Holford, J. Tessari, S. T. Mayne, P. H. Owens, B. Ward, D. Carter, P. Boyle, R. Dubrow, S. Archibeque-Engle, and S. H. Zahm, *Am. J. Epidemiol.*, **152**, 50 (2000).
2. L. Jarup, *Br. Med. Bull.*, **68**, 167 (2003).
3. S. Sounderajan, A. C. Udas, and B. Venkataramani, *J. Hazard. Mater.*, **149**, 238 (2007).
4. N. Zhang, N. Fu, Z. T. Fang, Y. H. Feng, and L. Ke, *Food Chem.* **124**, 1185 (2011).
5. S. Galani-Nikolaki, N. Kallithrakas-Kontos, and A. A. Katsanos, *Sci. Total Environ.*, **285**, 155 (2002).
6. R. A. Gil, N. Ferrua, J. A. Salonia, R. A. Olsina, and L. D. Martinez, *J. Hazard. Mater.*, **143**, 431 (2007).
7. L. Asensio, I. Gonzalez, T. Garcia, and R. Martin, *Food Control.* **19**, 1 (2008).
8. X. P. Yan, X. B. Yin, X. W. He, and Y. Jiang, *Anal. Chem.*, **74**, 2162 (2002).
9. Y. A. Vil’pan, I. L. Grinshtein, A. A. Akatov, and S. Gucer, *J. Anal. Chem.*, **60**, 38 (2005).
10. A. H. Huang, Z. G. Qiu, M. Jin, Z. Q. Shen, Z. L. Chen, X. W. Wang, and J. W. Li, *Int. J. Food Microbiol.*, **185**, 27 (2014).
11. A. Alishahi, H. Farahmand, N. Prieto, and D. Cozzolino, *Spectrochim. Acta A.*, **75**, 1 (2010).
12. J. K. Zheng and L. L. He, *Rev. Food. Sci. F.*, **13**, 317 (2014).
13. I. Choi, *J. Nanosci. Nanotechnol.*, **16**, 4274 (2016).
14. M. Li, S. K. Cushing, and N. Q. Wu, *Analyst*, **140**, 386 (2015).
15. J. L. Duan and J. H. Zhan, *Sci. China-Mater.*, **58**, 223 (2015).
16. M. Fleischmann, P. J. Hendra, and A. J. McQuillan, *Chem. Phys. Lett.*, **26**, 163 (1974).
17. A. J. McQuillan, *Notes. Rec. Roy. Soc.*, **63**, 105 (2009).
18. C. L. Haynes, C. R. Yonzon, X. Y. Zhang, and R. P. Van Duyne, *J. Raman Spectrosc.*, **36**, 471 (2005).
19. *Principles of Surface-Enhanced Raman Spectroscopy: And Related Plasmonic Effects*, E. C. LeRu and P. G. Etchegoin, Eds., Elsevier, Oxford, UK, (2009)
20. S. Y. Ding, E. M. You, Z. Q. Tian, and M. Moskovits, *Chem. Soc. Rev.*, **46**, 4042 (2017).
21. A. B. Zrimsek, N. H. Chiang, M. Mattei, S. Zaleski, M. O. McAnally, C. T. Chapman, A. I. Henry, G. C. Schatz, and R. P. Van Duyne, *Chem. Rev.*, **117**, 7583 (2017).
22. S. Jiang, Y. Zhang, R. Zhang, C. R. Hu, M. H. Liao, Y. Luo, J. L. Yang, Z. C. Dong, and J. G. Hou, *Nat. Nanotechnol.*, **10**, 865 (2015).
23. S. Pahlow, S. Meisel, D. Cialla-May, K. Weber, P. Rosch, and J. Popp, *Adv. Drug Delivery Rev.*, **89**, 105 (2015).
24. C. C. Fu, L. J. Liang, G. H. Qi, S. P. Xu, and W. Q. Xu, *Chem. J. Chinese U.*, **36**, 2134 (2015).
25. Y. S. Li and J. S. Church, *J. Food Drug Anal.*, **22**, 29 (2014).
26. J. H. Granger, N. E. Schlotter, A. C. Crawford, and M. D. Porter, *Chem. Soc. Rev.*, **45**, 3865 (2016).
27. Y. Liu, H. B. Zhou, Z. W. Hu, G. X. Yu, D. T. Yang, and J. S. Zhao, *Biosens. Bioelectron.*, **94**, 131 (2017).
28. Z. L. Sun, J. J. Du, and C. Y. Jing, *J. Environ. Sci.*, **39**, 134 (2016).
29. C. Y. Song, B. Y. Yang, Y. J. Yang, and L. H. Wang, *Sci. China-Chem.*, **59**, 16 (2016).
30. M. L. Xu, Y. Gao, X. X. Han, and B. Zhao, *J. Agric. Food Chem.*, **65**, 6719 (2017).
31. S. T. R. Pang, T. X. Yang, and L. L. He, *Trac-Trend Anal. Chem.*, **85**, 73 (2016).
32. J. M. Hao, M. J. Han, S. M. Han, X. G. Meng, T. L. Su, and Q. W. K. Wang, *J. Environ. Sci.*, **36**, 152 (2015).

33. J. M. Hao and X. G. Meng, *Front. Chem. Sci. Eng.*, **11**, 448 (2017).
34. T. Yang, H. F. Huang, F. Zhu, Q. L. Lin, L. Zhang, and J. W. Liu, *Sensors*, **16**, (2016).
35. A. P. Craig, A. S. Franca, and J. Irudayaraj, *Annu. Rev. Food Sci. T.*, **4**, 369 (2013).
36. S. D. Christesen, *Appl. Spectrosc.*, **42**, 318 (1988).
37. K. Kneipp, *J. Phys. Chem. C.*, **120**, 21076 (2016).
38. K. Kneipp, H. Kneipp, I. Itzkan, R. R. Dasari, and M. S. Feld, *Chem. Rev.*, **99**, 2957 (1999).
39. W. E. Doering and S. M. Nie, *J. Phys. Chem. B.*, **106**, 311 (2002).
40. P. L. Stiles, J. A. Dieringer, N. C. Shah, and R. R. Van Duyne, *Annu. Rev. Anal. Chem.*, **1**, 601 (2008).
41. M. Moskovits, *Rev. Mod. Phys.*, **57**, 783 (1985).
42. *Surface-Enhanced Raman Scattering: Physics and Applications*, K. Kneipp, M. Martin, and K. Harald, Eds., Springer-Verlag Berlin Heidelberg, Berlin, (2006).
43. E. C. Le Ru, E. Blackie, M. Meyer, and P. G. Etchegoin, *J. Phys. Chem. C.*, **111**, 13794 (2007).
44. E. C. Le Ru, J. Grand, I. Sow, W. R. C. Somerville, P. G. Etchegoin, M. Treguer-Delapierre, G. Charron, N. Felidi, G. Levi, and J. Aubard, *Nano Lett.*, **11**, 5013 (2011).
45. H. Y. Liang, Z. P. Li, W. Z. Wang, Y. S. Wu, and H. X. Xu, *Adv. Mater.*, **21**, 4614 (2009).
46. M. Li, S. K. Cushing, J. M. Zhang, J. Lankford, Z. P. Aguilar, D. L. Ma, and N. Q. Wu, *Nanotechnology*, **23**, (2012).
47. J. M. McMahon, S. Z. Li, L. K. Ausman, and G. C. Schatz, *J. Phys. Chem. C.*, **116**, 1627 (2012).
48. S. L. Kleinman, R. R. Frontiera, A. I. Henry, J. A. Dieringer, and R. P. Van Duyne, *Phys. Chem. Chem. Phys.*, **15**, 21 (2013).
49. D. K. Lim, K. S. Jeon, J. H. Hwang, H. Kim, S. Kwon, Y. D. Suh, and J. M. Nam, *Nat. Nanotechnol.*, **6**, 452 (2011).
50. D. K. Lim, K. S. Jeon, H. M. Kim, J. M. Nam, and Y. D. Suh, *Nat. Mater.*, **9**, 60 (2010).
51. H. X. Xu, J. Aizpurua, M. Kall, and P. Apell, *Phys. Rev. E*, **62**, 4318 (2000).
52. K. L. Wustholz, A. I. Henry, J. M. McMahon, R. G. Freeman, N. Valley, M. E. Piotti, M. J. Natan, G. C. Schatz, and R. P. Van Duyne, *J. Am. Chem. Soc.*, **132**, 10903 (2010).
53. J. P. Camden, J. A. Dieringer, Y. M. Wang, D. J. Masiello, L. D. Marks, G. C. Schatz, and R. P. Van Duyne, *J. Am. Chem. Soc.*, **130**, 12616 (2008).
54. P. H. C. Camargo, M. Rycenga, L. Au, and Y. N. Xia, *Angew. Chem. Int. Ed.*, **48**, 2180 (2009).
55. W. Y. Li, P. H. C. Camargo, X. M. Lu, and Y. N. Xia, *Nano Lett.*, **9**, 485 (2009).
56. S. M. Nie and S. R. Emery, *Science*, **275**, 1102 (1997).
57. K. Kneipp, Y. Wang, H. Kneipp, L. T. Perelman, I. Itzkan, R. Dasari, and M. S. Feld, *Phys. Rev. Lett.*, **78**, 1667 (1997).
58. K. Kneipp and H. Kneipp, *Appl. Spectrosc.*, **60**, 322a (2006).
59. Y. N. Xia, Y. J. Xiong, B. Lim, and S. E. Skrabalak, *Angew. Chem. Int. Ed.*, **48**, 60 (2009).
60. J. Zeng, Y. Q. Zheng, M. Rycenga, J. Tao, Z. Y. Li, Q. A. Zhang, Y. M. Zhu, and Y. N. Xia, *J. Am. Chem. Soc.*, **132**, 8552 (2010).
61. N. R. Jana, L. Gearheart, and C. J. Murphy, *Adv. Mater.*, **13**, 1389 (2001).
62. S. E. Lohse and C. J. Murphy, *Chem. Mater.*, **25**, 1250 (2013).
63. S. Si, W. Liang, Y. Sun, J. Huang, W. Ma, Z. Liang, Q. Bao, and L. Jiang, *Adv. Funct. Mater.*, **26**, 8137 (2016).
64. N. Zhou, G. Meng, Z. Huang, Y. Ke, Q. Zhou, and X. Hu, *Analyst*, **141**, 5864 (2016).
65. H. Wang, C. S. Levin, and N. J. Halas, *J. Am. Chem. Soc.*, **127**, 14992 (2005).
66. H.-Y. Chen, M.-H. Lin, C.-Y. Wang, Y.-M. Chang, and S. Gwo, *J. Am. Chem. Soc.*, **137**, 13698 (2015).
67. C. Hamon, S. Novikov, L. Scarabelli, L. Basabe-Desmonts, and L. M. Liz-Marzan, *ACS Nano*, **8**, 10694 (2014).
68. S. Gómez-Graña, C. Fernández-López, L. Polavarapu, J.-B. Salmon, J. Leng, I. Pastoriza-Santos, and J. Pérez-Juste, *Chem. Mater.*, **27**, 8310 (2015).
69. H. Liu, Z. Yang, L. Meng, Y. Sun, J. Wang, L. Yang, J. Liu, and Z. Tian, *J. Am. Chem. Soc.*, **136**, 5332 (2014).
70. Z. Li, G. Meng, Q. Huang, C. Zhu, Z. Zhang, and X. Li, *Chem-Eur. J.*, **18**, 14948 (2012).
71. C. Zhu, G. Meng, Q. Huang, and Z. Huang, *J. Hazard. Mater.*, **211**, 389 (2012).
72. C. Zhu, G. Meng, Q. Huang, Z. Li, Z. Huang, M. Wang, and J. Yuan, *J. Mater. Chem.*, **22**, 2271 (2012).
73. C. Zhu, G. Meng, Q. Huang, Y. Zhang, H. Tang, Y. Qian, B. Chen, and X. Wang, *Chem.-Eur. J.*, **19**, 9211 (2013).
74. Z. Huang, G. Meng, Q. Huang, Y. Yang, C. Zhu, and C. Tang, *Adv. Mater.*, **22**, 4136 (2010).
75. H. Tang, G. Meng, Z. Li, C. Zhu, Z. Huang, Z. Wang, and F. Li, *Nano Research*, **8**, 2261 (2015).
76. H. Tang, G. Meng, Q. Huang, C. Zhu, Z. Huang, Z. Li, Z. Zhanga, and Y. Zhang, *RSC Advances*, **4**, 19654 (2014).
77. Z. Huang, G. Meng, Q. Huang, B. Chen, C. Zhu, and Z. Zhang, *J. Raman Spectrosc.*, **44**, 240 (2013).
78. C. Hou, G. Meng, Z. Huang, B. Chen, C. Zhu, and Z. Li, *Electrochem. Commun.*, **60**, 104 (2015).
79. B. Chen, G. Meng, Q. Huang, Z. Huang, Q. Xu, C. Zhu, Y. Qian, and Y. Ding, *ACS Appl. Mater. Interfaces*, **6**, 15667 (2014).
80. S. J. Lee, A. R. Morrill, and M. Moskovits, *J. Am. Chem. Soc.*, **128**, 2200 (2006).
81. H. H. Wang, C. Y. Liu, S. B. Wu, N. W. Liu, C. Y. Peng, T. H. Chan, C. F. Hsu, J. K. Wang, and Y. L. Wang, *Adv. Mater.*, **18**, 491 (2006).
82. Q. Fu, Z. Zhan, J. Dou, X. Zheng, R. Xu, M. Wu, and Y. Lei, *ACS Appl. Mater. Interfaces.*, **7**, 13322 (2015).
83. H. Tang, P. Zheng, G. Meng, Z. Li, C. Zhu, F. Han, Y. Ke, Z. Wang, F. Zhou, and N. Wu, *Nanotechnology*, **27**, (2016).
84. K. Sun, G. Meng, Q. Huang, X. Zhao, C. Zhu, Z. Huang, Y. Qian, X. Wang, and X. Hu, *J. Mater. Chem. C.*, **1**, 5015 (2013).
85. C. Zhu, G. Meng, P. Zheng, Q. Huang, Z. Li, X. Hu, X. Wang, Z. Huang, F. Li, and N. Wu, *Adv. Mater.*, **28**, 4871 (2016).
86. S. S. Masango, R. A. Hackler, N. Large, A.-I. Henry, M. O. McAnally, G. C. Schatz, P. C. Stair, and R. P. Van Duyne, *Nano Lett.*, **16**, 4251 (2016).
87. S. Yang, W. Cai, L. Kong, and Y. Lei, *Adv. Funct. Mater.*, **20**, 2527 (2010).
88. H. Ni, M. Wang, T. Shen, and J. Zhou, *ACS Nano*, **9**, 1913 (2015).
89. A. Sánchez-Iglesias, P. Aldeanueva-Potel, W. Ni, J. Pérez-Juste, I. Pastoriza-Santos, R. A. Alvarez-Puebla, B. N. Mbenkum, and L. M. Liz-Marzán, *Nano Today*, **5**, 21 (2010).
90. J. Zuo, G. Meng, C. Zhu, Q. Zhou, Z. Li, Y. Ke, and N. Zhou, *RSC Advances*, **6**, 26490 (2016).
91. T. Y. Jeon, S.-G. Park, D.-H. Kim, and S.-H. Kim, *Adv. Funct. Mater.*, **25**, 4681 (2015).
92. H. C. Jeon, T. Y. Jeon, T. S. Shim, and S.-M. Yang, *Small*, **10**, 1490 (2014).
93. H. C. Jeon, C.-J. Heo, S. Y. Lee, and S.-M. Yang, *Adv. Funct. Mater.*, **22**, 4268 (2012).
94. Q. Zhang, Y. H. Lee, I. Y. Phang, C. K. Lee, and X. Y. Ling, *Small*, **10**, 2703 (2014).
95. A. Gopalakrishnan, M. Chirumamilla, F. De Angelis, A. Toma, R. P. Zaccaria, and R. Krahne, *ACS Nano*, **8**, 7986 (2014).
96. W. Xu, X. Ling, J. Xiao, M. S. Dresselhaus, J. Kong, H. Xu, Z. Liu, and J. Zhang, *Proc. Natl. Acad. Sci. U. S. A.*, **109**, 9281 (2012).
97. Y.-J. Oh and K.-H. Jeong, *Adv. Mater.*, **24**, 2234 (2012).
98. Q. Zhou, G. Meng, Q. Huang, C. Zhu, H. Tang, Y. Qian, B. Chen, and B. Chen, *Phys. Chem. Chem. Phys.*, **16**, 3686 (2014).
99. S. Lee, M. G. Hamm, R. Vajtai, D. P. Hashim, T. Thurakitserree, A. C. Chipara, P. M. Ajayan, and J. H. Hafner, *Adv. Mater.*, **24**, 5261 (2012).
100. B. Zhang, H. Wang, L. Lu, K. Ai, G. Zhang, and X. Cheng, *Adv. Funct. Mater.*, **18**, 2348 (2008).
101. J. Liu, G. Meng, X. Li, and Z. Huang, *Langmuir*, **30**, 13964 (2014).
102. L. Xue, W. Xie, L. Driessen, K. F. Domke, Y. Wang, S. Schlucker, S. N. Gorb, and M. Steinhart, *Small*, **13**, (2017).
103. R. Kodiyath, J. Wang, Z. A. Combs, S. Chang, M. K. Gupta, K. D. Anderson, R. J. C. Brown, and V. V. Tsukruk, *Small*, **7**, 3452 (2011).
104. Y. Qian, G. Meng, Q. Huang, C. Zhu, Z. Huang, K. Sun, and B. Chen, *Nanoscale*, **6**, 4781 (2014).
105. X. Hu, G. Meng, Q. Huang, C. Zhu, B. Chen, Z. Huang, F. Li, and Z. Wang, *ACS Appl. Mater. Interfaces*, **6**, 7991 (2014).
106. P. D. Nallathambi, T. Huang, and X. H. N. Xu, *Nanoscale*, **2**, 1715 (2010).
107. H. Baida, P. Billaud, S. Marhaba, D. Christofilos, E. Cottancin, A. Crut, J. Lerne, P. Maioli, M. Pellarin, M. Broyer, N. Del Fatti, F. Vallee, A. Sanchez-Iglesias, I. Pastoriza-Santos, and L. M. Liz-Marzan, *Nano Lett.*, **9**, 3463 (2009).
108. T. Huang and X. H. N. Xu, *J. Mater. Chem.*, **20**, 9867 (2010).
109. J. Cao, T. Sun, and K. T. V. Grattan, *Sens. Actuator B-Chem.*, **195**, 332 (2014).
110. V. Juve, M. F. Cardinal, A. Lombardi, A. Crut, P. Maioli, J. Perez-Juste, L. M. Liz-Marzan, N. Del Fatti, and F. Vallee, *Nano Lett.*, **13**, 2234 (2013).
111. L. Tong, Q. S. Wei, A. Wei, and J. X. Cheng, *Photochem. Photobiol.*, **85**, 21 (2009).
112. Z. Yang, M. Q. Wang, G. D. Yan, X. Y. Zhang, and J. J. Ding, *2013 13th IEEE Conference on Nanotechnology (Ieee-Nano)*, 280 (2013).
113. X. H. Huang, I. H. El-Sayed, W. Qian, and M. A. El-Sayed, *J. Am. Chem. Soc.*, **128**, 2115 (2006).
114. M. R. K. Ali, B. Snyder, and M. A. El-Sayed, *Langmuir*, **28**, 9807 (2012).
115. S. W. Prescott and P. Mulvaney, *J. Appl. Phys.*, **99**, 123504 (2006).
116. C. J. Orendorff and C. J. Murphy, *J. Phys. Chem. B.*, **110**, 3990 (2006).
117. C. Rehbock, J. Jakobi, L. Gamrad, S. van der Meer, D. Tiedemann, U. Taylor, W. Kues, D. Rath, and S. Barcikowski, *Beilstein J. Nanotech.*, **5**, 1523 (2014).
118. D. Tiedemann, U. Taylor, C. Rehbock, J. Jakobi, S. Klein, W. A. Kues, S. Barcikowski, and D. Rath, *Analyst*, **139**, 931 (2014).
119. P. Zheng, S. K. Cushing, S. Suri, and N. Q. Wu, *Phys. Chem. Chem. Phys.*, **17**, 21211 (2015).
120. T. W. Clarkson, L. Magos, and G. J. Myers, *N. Engl. J. Med.*, **349**, 1731 (2003).
121. *National Primary Drinking Water Regulations*. Available from: <https://www.epa.gov/ground-water-and-drinking-water/national-primary-drinking-water-regulations#one>.
122. R. Wittman and H. Hu, *Environ. Health Perspect.*, **110**, 1261 (2002).
123. E. Vetrinurugan, K. Brindha, L. Elango, and O. M. Ndwandwe, *Appl. Water Sci.*, **7**, 3267 (2017).
124. D. Mohan and C. U. Pittman, *J. Hazard. Mater.*, **142**, 1 (2007).
125. S. Fendorf, H. A. Michael, and A. van Geen, *Science*, **328**, 1123 (2010).
126. I. Onyido, A. R. Norris, and E. Bunzel, *Chem. Rev.*, **104**, 5911 (2004).
127. *Learn about Lead*. Available from: <https://www.epa.gov/lead/learn-about-lead>.
128. P. M. Vitousek, J. D. Aber, R. W. Howarth, G. E. Likens, P. A. Matson, D. W. Schindler, W. H. Schlesinger, and D. Tilman, *Ecol. Appl.*, **7**, 737 (1997).
129. A. Srinivasan and T. Viraraghavan, *Int. J. Environ. Res. Public Health.*, **6**, 1418 (2009).
130. *Health aspects of plumbing*, World Health Organization and World Plumbing Council Eds., World Health Organization, Geneva, (2006)
131. FDA. *2004–2005 Exploratory Survey Data on Perchlorate in Food*. Available from: <https://www.fda.gov/Food/FoodborneIllnessContaminants/ChemicalContaminants/ucm077685.htm>.
132. ATSDR. *Nitrate/Nitrite Toxicity What Are U. S. Standards and Regulations for Nitrates and Nitrites Exposure*. Available from: <https://www.atsdr.cdc.gov/csem/csem.asp?csem=28&po=8>.

133. R. A. Alvarez-Puebla and L. M. Liz-Marzan, *Angew. Chem. Int. Ed.*, **51**, 11214 (2012).
134. Z. H. Xu, C. Y. Jing, J. M. Hao, C. Christodoulatos, G. P. Korfiatis, F. S. Li, and X. G. Meng, *J. Phys. Chem. C.*, **116**, 325 (2012).
135. M. Mulvihill, A. Tao, K. Benjauthrit, J. Arnold, and P. Yang, *Angew. Chem. Int. Ed.*, **47**, 6456 (2008).
136. L. L. Bao, S. M. Mahurin, R. G. Haire, and S. Dai, *Anal. Chem.*, **75**, 6614 (2003).
137. D. Bhandari, S. M. Wells, S. T. Retterer, and M. J. Sepaniak, *Anal. Chem.*, **81**, 8061 (2009).
138. J. M. Hao, Z. H. Xu, M. J. Han, S. Y. Xu, and X. G. Meng, *Colloid Surface A*, **366**, 163 (2010).
139. S. Gajaraj, C. Fan, M. S. Lin, and Z. Q. Hu, *Environ. Monit. Assess.*, **185**, 5673 (2013).
140. C. M. Ruan, W. Wang, and A. H. Gu, *Anal. Chim. Acta.*, **567**, 114 (2006).
141. B. H. Gu, C. M. Ruan, and W. Wang, *Appl. Spectrosc.*, **63**, 98 (2009).
142. S. Tan, M. Erol, S. Sukhishvili, and H. Du, *Langmuir*, **24**, 4765 (2008).
143. V. M. Zamarion, R. A. Timm, K. Araki, and H. E. Toma, *Inorg. Chem.*, **47**, 2934 (2008).
144. L. Guerrini, I. Rodriguez-Loureiro, M. A. Correa-Duarte, Y. H. Lee, X. Y. Ling, F. J. G. de Abajo, and R. A. Alvarez-Puebla, *Nanoscale*, **6**, 8368 (2014).
145. N. H. Ly and S. W. Joo, *Bull. Korean Chem. Soc.*, **36**, 226 (2015).
146. Y. Zhao, J. N. Newton, J. Liu, and A. Wei, *Langmuir*, **25**, 13833 (2009).
147. S. Sarkar, M. Pradhan, A. K. Sinha, M. Basu, and T. Pal, *Chem-Eur. J.*, **18**, 6335 (2012).
148. W. Q. Tang, D. B. Chase, D. L. Sparks, and J. F. Rabolt, *Appl. Spectrosc.*, **69**, 843 (2015).
149. Y. X. Yuan, L. Ling, X. Y. Wang, M. Wang, R. A. Gu, and J. L. Yao, *J. Raman Spectrosc.*, **38**, 1280 (2007).
150. S. J. Lee and M. Moskovits, *Nano Lett.*, **11**, 145 (2011).
151. O. Guselnikova, P. Postnikov, M. Erzina, Y. Kalachyova, V. Svorcik, and O. Lyutakov, *Sensors Actuat. B-Chem.*, **253**, 830 (2017).
152. J. L. Li, L. X. Chen, T. T. Lou, and Y. Q. Wang, *ACS Appl. Mater. Interfaces*, **3**, 3936 (2011).
153. J. Yin, T. Wu, J. B. Song, Q. Zhang, S. Y. Liu, R. Xu, and H. W. Duan, *Chem. Mater.*, **23**, 4756 (2011).
154. F. Li, J. Wang, Y. M. Lai, C. Wu, S. Q. Sun, Y. H. He, and H. Ma, *Biosens. Bioelectron.*, **39**, 82 (2013).
155. Y. Zeng, L. H. Wang, L. W. Zeng, A. G. Shen, and J. M. Hu, *Talanta*, **162**, 374 (2017).
156. M. P. Cecchini, V. A. Turek, A. Demetriadou, G. Britovsek, T. Welton, A. A. Kornyshev, J. D. E. T. Wilton-Ely, and J. B. Edel, *Adv. Opt. Mater.*, **2**, 966 (2014).
157. X. F. Wang, Y. H. Shen, A. J. Xie, and S. H. Chen, *Mater. Chem. Phys.*, **140**, 487 (2013).
158. Y. Kang, T. Wu, B. X. Liu, X. Wang, and Y. P. Du, *Microchim. Acta.*, **181**, 1333 (2014).
159. P. Zheng, X. F. Shi, K. Curtin, F. Yang, and N. Q. Wu, *Mater. Res. Express*, **4**, (2017).
160. W. Zhou, B. C. Yin, and B. C. Ye, *Biosens. Bioelectron.*, **87**, 187 (2017).
161. S. Li, L. G. Xu, W. Ma, H. Kuang, L. B. Wang, and C. L. Xu, *Small*, **11**, 3435 (2015).
162. W. Ma, M. Z. Sun, L. G. Xu, L. B. Wang, H. Kuang, and C. L. Xu, *Chem. Commun.*, **49**, 4989 (2013).
163. P. Zheng, M. Li, R. Jurevic, S. K. Cushing, Y. X. Liu, and N. Q. Wu, *Nanoscale*, **7**, 11005 (2015).
164. D. Han, S. Y. Lim, B. J. Kim, L. Piao, and T. D. Chung, *Chem. Commun.*, **46**, 5587 (2010).
165. B. Sun, X. X. Jiang, H. Y. Wang, B. Song, Y. Zhu, H. Wang, Y. Y. Su, and Y. He, *Anal. Chem.*, **87**, 1250 (2015).
166. T. Senapati, D. Senapati, A. K. Singh, Z. Fan, R. Kanchanapally, and P. C. Ray, *Chem. Commun.*, **47**, 10326 (2011).
167. Y. X. Du, R. Y. Liu, B. H. Liu, S. H. Wang, M. Y. Han, and Z. P. Zhang, *Anal. Chem.*, **85**, 3160 (2013).
168. Y. H. Luo, K. Li, G. Q. Wen, Q. Y. Liu, A. H. Liang, and Z. L. Jiang, *Plasmonics*, **7**, 461 (2012).
169. P. Li, H. L. Liu, L. B. Yang, and J. H. Liu, *Talanta*, **106**, 381 (2013).
170. P. Y. Ma, F. H. Liang, Q. Q. Yang, D. Wang, Y. Sun, X. H. Wang, D. J. Gao, and D. Q. Song, *Microchim. Acta.*, **181**, 975 (2014).
171. Y. Chen, L. H. Wu, Y. H. Chen, N. Bi, X. Zheng, H. B. Qi, M. H. Qin, X. Liao, H. Q. Zhang, and Y. Tian, *Microchim. Acta.*, **177**, 341 (2012).
172. E. Chung, R. Gao, J. Ko, N. Choi, D. W. Lim, E. K. Lee, S. I. Chang, and J. Choo, *Lab Chip*, **13**, 260 (2013).
173. T. Kang, S. M. Yoo, M. Kang, H. Lee, H. Kim, S. Y. Lee, and B. Kim, *Lab Chip*, **12**, 3077 (2012).
174. Y. L. Wang and J. Irudayaraj, *Chem. Commun.*, **47**, 4394 (2011).
175. H. Kim, T. Kang, H. Lee, H. Ryoo, S. M. Yoo, S. Y. Lee, and B. Kim, *Chem-Asian J.*, **8**, 3010 (2013).
176. L. Y. Zhao, W. Gu, C. L. Zhang, X. H. Shi, and Y. Z. Xian, *J. Colloid Interface Sci.*, **465**, 279 (2016).
177. G. Wang, C. Lim, L. Chen, H. Chon, J. Choo, J. Hong, and A. J. deMello, *Anal. Bioanal. Chem.*, **394**, 1827 (2009).
178. S. Y. Fu, X. Y. Guo, H. Wang, T. X. Yang, Y. Wen, and H. F. Yang, *Sensors Actuat. B-Chem.*, **199**, 108 (2014).
179. W. Ren, C. Z. Zhu, and E. K. Wang, *Nanoscale*, **4**, 5902 (2012).
180. W. Ji, L. Chen, X. X. Xue, Z. N. Guo, Z. Yu, B. Zhao, and Y. Ozaki, *Chem. Commun.*, **49**, 7334 (2013).
181. C. Wang, S. Wu, S. Zhou, Y. Shi, and J. Song, *Pedosphere*, **27**, 17 (2017).
182. A. S. Tsiabart and A. N. Gennadiev, *Eurasian Soil Science*, **46**, 728 (2013).
183. S. O. Baek, R. A. Field, M. E. Goldstone, P. W. Kirk, J. N. Lester, and R. Perry, *Water Air Soil Pollut.*, **60**, 279 (1991).
184. K. Ravindra, R. Sokhi, and R. Vangrieken, *Atmos. Environ.*, **42**, 2895 (2008).
185. K. Ravindra, R. Sokhi, and R. Van Grieken, *Atmos. Environ.*, **42**, 2895 (2008).
186. J. P. Incardona, T. K. Collier, and N. L. Scholz, *Toxicol. Appl. Pharmacol.*, **196**, 191 (2004).
187. A. Ramesh, S. A. Walker, D. B. Hood, M. D. Guillen, K. Schneider, and E. H. Weyand, *Int. J. Toxicol.*, **23**, 301 (2004).
188. M. D. Pereira, *Quim. Nova.*, **27**, 934 (2004).
189. U. S. E. P. Agency. *Learn about Polychlorinated Biphenyls (PCBs)*. Available from: <https://www.epa.gov/pcbs/learn-about-polychlorinated-biphenyls-pcbs#healtheffects>.
190. EPA. *Basic Information about Pesticide Ingredients*. Available from: <https://www.epa.gov/ingredients-used-pesticide-products/basic-information-about-pesticide-ingredients>.
191. WHO. *Issue Brief Series: Pesticides*. Available from: <http://www.who.int/heca/infomaterials/pesticides.pdf?ua=1>.
192. L. An and W. Sun, *Neurotox. Res.*, **32**, 301 (2017).
193. J. F. Li, Y. F. Huang, Y. Ding, Z. L. Yang, S. B. Li, X. S. Zhou, F. R. Fan, W. Zhang, Z. Y. Zhou, D. Y. Wu, B. Ren, Z. L. Wang, and Z. Q. Tian, *Nature*, **464**, 392 (2010).
194. Q. T. Zhou, G. W. Meng, N. Q. Wu, N. N. Zhou, B. S. Chen, F. D. Li, and Q. Huang, *Sensors Actuat. B-Chem.*, **223**, 447 (2016).
195. N. N. Zhou, Q. T. Zhou, G. W. Meng, Z. L. Huang, Y. Ke, J. Liu, and N. Q. Wu, *Acs Sensors*, **1**, 1193 (2016).
196. A. Kim, S. J. Barcelo, R. S. Williams, and Z. Y. Li, *Anal. Chem.*, **84**, 9303 (2012).
197. Z. Li, G. Meng, Q. Huang, X. Hu, X. He, H. Tang, Z. Wang, and F. Li, *Small*, **11**, 5452 (2015).
198. J. Ma, D. D. Kong, X. H. Han, W. L. Guo, and X. F. Shi, *Spectrosc. Spect. Anal.*, **33**, 2688 (2013).
199. L. L. He, M. S. Lin, H. Li, and N. J. Kim, *J. Raman Spectrosc.*, **41**, 739 (2010).
200. H. Tang, G. Meng, Q. Huang, Z. Zhang, Z. Huang, and C. Zhu, *Adv. Funct. Mater.*, **22**, 218 (2012).
201. Y. J. Yang and G. W. Meng, *J. Appl. Phys.*, **107**, (2010).
202. Q. Deng, H. B. Tang, G. Liu, X. P. Song, S. H. Kang, H. M. Wang, D. H. L. Ng, and G. Z. Wang, *New J. Chem.*, **39**, 7781 (2015).
203. K. C. Bantz and C. L. Haynes, *Vib. Spectrosc.*, **50**, 29 (2009).
204. K. C. Bantz, H. D. Nelson, and C. L. Haynes, *J. Phys. Chem. C*, **116**, 3585 (2012).
205. Y. H. Kwon, K. Sowoidnich, H. Schmidt, and H. D. Kronfeldt, *J. Raman Spectrosc.*, **43**, 1003 (2012).
206. P. Liu, D. Zhang, and J. Zhan, *J. Phys. Chem. A.*, **114**, 13122 (2010).
207. J. Yuan, Y. Lai, J. Duan, Q. Zhao, and J. Zhan, *J. Colloid Interface Sci.*, **365**, 122 (2012).
208. B. Chen, G. Meng, F. Zhou, Q. Huang, C. Zhu, X. Hu, and M. Kong, *Nanotechnology*, **25**, (2014).
209. Y. L. Lu, G. H. Yao, K. X. Sun, and Q. Huang, *Phys. Chem. Chem. Phys.*, **17**, 21149 (2015).
210. C. H. Zhu, X. J. Wang, X. F. Sho, F. Yang, G. W. Meng, Q. H. Xiong, Y. Ke, H. Wang, Y. L. Lu, and N. Q. Wu, *ACS Appl. Mater. Interfaces*, **9**, 39618 (2017).
211. L. E. Kreno, N. G. Greeneltch, O. K. Farha, J. T. Hupp, and R. P. Van Duyne, *The Analyst*, **139**, 4073 (2014).
212. Y. L. Hu, J. Liao, D. M. Wang, and G. K. Li, *Anal. Chem.*, **86**, 3955 (2014).
213. Q. Zhou, G. Meng, J. Liu, Z. Huang, F. Han, C. Zhu, D.-J. Kim, T. Kim, and N. Wu, *Adv. Mater. Technol.*, **2**, 1700028 (2017).
214. D. Li, D. W. Li, J. S. Fossey, and Y. T. Long, *Anal. Chem.*, **82**, 9299 (2010).
215. Y. T. Li, L. L. Qu, D. W. Li, Q. X. Song, F. Fathi, and Y. T. Long, *Biosens. Bioelectron.*, **43**, 94 (2013).
216. R. A. Alvarez-Puebla, R. Contreras-Caceres, I. Pastoriza-Santos, J. Pérez-Juste, and L. M. Liz-Marzan, *Angew. Chem. Int. Ed.*, **48**, 138 (2009).
217. Q. Zhou, G. Meng, P. Zheng, S. Cushing, N. Wu, Q. Huang, C. Zhu, Z. Zhang, and Z. Wang, *Sci. Rep.*, **5**, (2015).
218. Z. Huang, G. Meng, Q. Huang, B. Chen, F. Zhou, X. Hu, Y. Qian, H. Tang, F. Han, and Z. Chu, *Nano Research*, **7**, 1177 (2014).
219. L. Yang, L. Ma, G. Chen, J. Liu, and Z.-Q. Tian, *Chem-A Eur. J.*, **16**, 12683 (2010).
220. M. M. Liu and W. Chen, *Biosens. Bioelectron.*, **46**, 68 (2013).
221. N. Chen, P. Ding, Y. Shi, T. Y. Jin, Y. Y. Su, H. Y. Wang, and Y. He, *Anal. Chem.*, **89**, 5072 (2017).
222. K. Sun, Q. Huang, G. Meng, and Y. Lu, *ACS Appl. Mater. Interfaces*, **8**, 5723 (2016).
223. Y. Lu, Q. Huang, G. Meng, L. Wu, and Z. Jingjing, *The Analyst*, **139**, 3083 (2014).
224. M. Li, J. Zhang, S. Suri, L. J. Sooter, D. Ma, and N. Wu, *Anal. Chem.*, **84**, 2837 (2012).
225. NIH and NIAID. *NIAID Emerging Infectious Diseases/Pathogens*. Available from: <https://www.niaid.nih.gov/research/emerging-infectious-diseases-pathogens>.
226. Centers for Disease Control and Prevention. *Burden of Foodborne Illness: Overview*. 2011; Available from: <https://www.cdc.gov/foodborneburden/estimates-overview.html>.
227. Healthline. *Worst Foodborne Illness Outbreaks in Recent U. S. History*. Available from: <https://www.healthline.com/health/worst-foodborne-illness-outbreaks>.
228. H. W. Cheng, S. Y. Huan, and R. Q. Yu, *Analyst*, **137**, 3601 (2012).
229. X. Y. Zhang, N. C. Shah, and R. P. Van Duyne, *Vib. Spectrosc.*, **42**, 2 (2006).
230. X. Y. Zhang, M. A. Young, O. Lyandres, and R. P. Van Duyne, *J. Am. Chem. Soc.*, **127**, 4484 (2005).
231. D. P. Cowcher, Y. Xu, and R. Goodacre, *Anal. Chem.*, **85**, 3297 (2013).
232. R. M. Jarvis, N. Law, L. T. Shadi, P. O'Brien, J. R. Lloyd, and R. Goodacre, *Anal. Chem.*, **80**, 6741 (2008).

233. C. Fan, Z. Q. Hu, A. Mustapha, and M. S. Lin, *Appl. Microbiol. Biotechnol.*, **92**, 1053 (2011).
234. M. Kahraman, K. Keseroglu, and M. Culha, *Appl. Spectrosc.*, **65**, 500 (2011).
235. H. B. Zhou, D. T. Yang, N. P. Ivleva, N. E. Mircescu, R. Niessner, and C. Haisch, *Anal. Chem.*, **86**, 1525 (2014).
236. C. Fan, Z. Q. Hu, L. K. Riley, G. A. Purdy, A. Mustapha, and M. S. Lin, *J. Food Sci.*, **75**, M302 (2010).
237. S. Shanmukh, L. Jones, J. Driskell, Y. P. Zhao, R. Dluhy, and R. A. Tripp, *Nano Lett.*, **6**, 2630 (2006).
238. S. Shanmukh, L. Jones, Y. P. Zhao, J. D. Driskell, R. A. Tripp, and R. A. Dluhy, *Anal. Bioanal. Chem.*, **390**, 1551 (2008).
239. H. Y. Lin, C. H. Huang, W. H. Hsieh, L. H. Liu, Y. C. Lin, C. C. Chu, S. T. Wang, I. T. Kuo, L. K. Chau, and C. Y. Yang, *Small*, **10**, 4700 (2014).
240. X. Y. Ma, X. M. Xu, Y. Xia, and Z. P. Wang, *Food Control*, **84**, 232 (2018).
241. H. Zhang, X. Y. Ma, Y. Liu, N. Duan, S. J. Wu, Z. P. Wang, and B. C. Xu, *Biosens. Bioelectron.*, **74**, 872 (2015).
242. J. Neng, M. H. Harpster, W. C. Wilson, and P. A. Johnson, *Biosens. Bioelectron.*, **41**, 316 (2013).
243. D. H. Lin, T. Q. Qin, Y. Q. Wang, X. Y. Sun, and L. X. Chen, *ACS Appl. Mater. Interfaces*, **6**, 1320 (2014).
244. B. Guven, N. Basaran-Akgul, E. Temur, U. Tamer, and I. H. Boyaci, *Analyst*, **136**, 740 (2011).
245. S. A. Khan, A. K. Singh, D. Senapati, Z. Fan, and P. C. Ray, *Chem. Commun.*, **47**, 9444 (2011).
246. B. Pearson, P. X. Wang, A. Mills, S. T. R. Pang, L. McLandsborough, and L. L. He, *Anal. Methods*, **9**, 4732 (2017).
247. L. Yao, Y. W. Ye, J. Teng, F. D. Xue, D. G. Pan, B. G. Li, and W. Chen, *Anal. Chem.*, **89**, 9775 (2017).
248. M. Li, S. K. Cushing, H. Liang, S. Suri, D. Ma, and N. Wu, *Anal. Chem.*, **85**, 2072 (2013).
249. H. B. Pu, W. Xiao, and D. W. Sun, *Trends Food Sci. Technol.*, **70**, 114 (2017).
250. M. Zarei, *Biosens. Bioelectron.*, **98**, 494 (2017).
251. I. J. Jahn, O. Zukovskaja, X. S. Zheng, K. Weber, T. W. Bocklitz, D. Cialla-May, and J. Popp, *Analyst*, **142**, 1022 (2017).
252. A. F. Chrimes, K. Khoshmanesh, P. R. Stoddart, A. Mitchell, and K. Kalantar-zadeh, *Chem. Soc. Rev.*, **42**, 5880 (2013).
253. H. B. Liu, X. J. Du, Y. X. Zang, P. Li, and S. Wang, *J. Agric. Food Chem.*, **65**, 10290 (2017).
254. J. J. Liang, H. W. Liu, C. F. Lan, Q. Q. Fu, C. H. Huang, Z. Luo, T. J. Jiang, and Y. Tang, *Nanotechnology*, **25**, (2014).
255. J. Hwang, S. Lee, and J. Choo, *Nanoscale*, **8**, 11418 (2016).
256. L. Zhang, Y. J. Huang, J. Y. Wang, Y. Rong, W. H. Lai, J. W. Zhang, and T. Chen, *Langmuir*, **31**, 5537 (2015).
257. X. Fu, Z. Cheng, J. Yu, P. Choo, L. Chen, and J. Choo, *Biosens. Bioelectron.*, **78**, 530 (2016).
258. X. F. Gao, P. Zheng, S. Kasani, S. Wu, F. Yang, S. Lewis, S. Nayeem, E. B. Engler-Chiurazzi, J. G. Wigginton, J. W. Simpkins, and N. Q. Wu, *Anal. Chem.*, **89**, 10104 (2017).
259. A. Gunther, M. Jhunjunwala, M. Thalmann, M. A. Schmidt, and K. F. Jensen, *Langmuir*, **21**, 1547 (2005).
260. N. Choi, J. Lee, J. Ko, J. H. Jeon, G. Rhie, A. J. Demello, and J. Choo, *Anal. Chem.*, **89**, 8413 (2017).
261. N. Qi, B. W. Li, H. Y. You, W. Zhang, L. W. Fu, Y. Q. Wang, and L. X. Chen, *Anal. Methods*, **6**, 4077 (2014).
262. Q. Q. Fu, H. W. L. Liu, Z. Wu, A. Liu, C. Z. Yao, X. Q. Li, W. Xiao, S. T. Yu, Z. Luo, and Y. Tang, *J. Nanobiotechnol.*, **13**, (2015).
263. H. Z. Guo, Y. Z. Chen, M. B. Cortie, X. Liu, Q. S. Xie, X. Wang, and D. L. Peng, *J. Phys. Chem. C*, **118**, 9801 (2014).
264. I. Pastoriza-Santos, A. Sanchez-Iglesias, B. Rodriguez-Gonzalez, and L. M. Liz-Marzan, *Small*, **5**, 440 (2009).
265. H. J. Yang, S. Y. He, H. L. Chen, and H. Y. Tuan, *Chem. Mater.*, **26**, 1785 (2014).
266. C. C. Crane, F. Wang, J. Li, J. Tao, Y. M. Zhu, and J. Y. Chen, *J. Phys. Chem. C*, **121**, 5684 (2017).
267. M. W. Knight, N. S. King, L. Liu, H. O. Everitt, P. Nordlander, and N. J. Halas, *ACS Nano*, **8**, 834 (2014).
268. X. Tan, L. Wang, C. Cheng, X. Yan, B. Shen, and J. Zhang, *Chem. Comm.*, **52**, 2893 (2016).
269. T. Zheng, W. Sang, Z. He, Q. Wei, B. Chen, H. Li, C. Cao, R. Huang, X. Yan, B. Pan, S. Zhou, and J. Zeng, *Nano Lett.*, **17**, 7968 (2017).
270. J. Yan, T. Wang, G. Wu, W. Dai, N. Guan, L. Li, and J. Gong, *Adv. Mater.*, **27**, 1580 (2015).
271. A. Agrawal, S. H. Cho, O. Zandi, S. Ghosh, R. W. Johns, and D. J. Milliron, *Chem. Rev.*, **118**, 3121 (2018).
272. M. Li, S. K. Cushing, J. M. Zhang, S. Suri, R. Evans, W. P. Petros, L. F. Gibson, D. L. Ma, Y. X. Liu, and N. Q. Wu, *ACS Nano*, **7**, 4967 (2013).
273. S. Ayas, A. Cupallari, O. O. Ekiz, Y. Kaya, and A. Dana, *ACS Photonics*, **1**, 17 (2014).
274. Q. S. Wei, R. Nagi, K. Sadeghi, S. Feng, E. Yan, S. J. Ki, R. Caire, D. Tseng, and A. Ozcan, *ACS Nano*, **8**, 1121 (2014).
275. R. D. Munje, S. Muthukumar, and S. Prasad, *Sensor Actuat B-Chem.*, **238**, 482 (2017).
276. M. Zarei, *Trac-Trends in Anal. Chem.*, **91**, 26 (2017).
277. A. K. Yetisen, M. S. Akram, and C. R. Lowe, *Lab Chip*, **13**, 2210 (2013).